

Projected future changes in extreme precipitation over China under stratospheric aerosol intervention in the UKESM1 climate model

Ou Wang¹, Ju Liang², Yuchen Gu³, Jim M. Haywood^{4,5*}, Ying Chen⁶, Chenwei Fang⁷, Qin`geng Wang^{1*}

¹State Key Laboratory of Pollution Control and Resources Reuse, School of Environment, Nanjing University, Nanjing, 210023, China

²Department of Agricultural Meteorology, College of Resources and Environmental Sciences, China Agriculture University, Beijing 100193, China

³Department of Earth Science, Mathematical and Physical Sciences, University College London, London WC1E 6BT, UK

⁴~~Department of Mathematics, Faculty Dept of Mathematics, School~~ of Environment, Science and the Economy, University of Exeter, Exeter EX4 4QE, UK

⁵Met Office Hadley Centre, Exeter EX1 3PB, UK

⁶School of Geography Earth and Environment Sciences, University of Birmingham, Birmingham B15 2TT, UK

⁷Key Laboratory of Meteorological Disaster, Ministry of Education (KLME), Joint International Research Laboratory of Climate and Environment Change (ILCEC), Collaborative Innovation Centre on Forecast and Evaluation of Meteorological Disasters, Key Laboratory for Aerosol-Cloud-Precipitation of China Meteorological Administration, Nanjing University of Information Science & Technology, Nanjing, 210044, China

Correspondence to: [Qin`geng Wang \(wangqg@nju.edu.cn\)](mailto:wangqg@nju.edu.cn), [Jim M. Haywood \(J.M.Haywood@exeter.ac.uk\)](mailto:J.M.Haywood@exeter.ac.uk)

[Ou Wang \(dg1925035@smail.nju.edu.cn\)](mailto:dg1925035@smail.nju.edu.cn)

Abstract. Extreme precipitation events are linked to severe economic losses and casualties in China every year; hence, exploring the potential mitigation strategies to minimize these events and their changes in frequency and intensity under global warming is of importance, particularly for the populous subregions. In addition to global warming scenarios, this study examines the effects of the potential deployment of stratospheric aerosol injection (SAI) on hydrological extremes in China based on the SAI simulations (G6sulfur) of the Geoengineering Model Intercomparison Project (GeoMIP) by the UK Earth System Model (UKESM1)~~from UKESM1 (The UK Earth System Model)~~ simulations. The ~~G6sulfur simulated SAI deployment~~ is compared with simulations of the future climate under two different emission scenarios (SSP5-8.5 and SSP2-4.5) and reduction in the solar constant (G6solar) to understand the effect of SAI on extreme precipitation patterns. The results show that, under future ~~global warming scenarios simulations~~ (SSP5-8.5 and SSP2-4.5), precipitation and extreme wet climate events during 2071-2100 are projected to increase ~~by 2100~~ relative to the control period (1981-2010)~~present day~~ across all the subregions in China. ~~Additionally, analyses of e~~Extreme drought events show a projected increase in southern China. The G6sulfur and G6solar experiments ameliorate the increases in extreme rainfall intensities, especially for the eastern subregions of China. The ~~efficacy impacts~~ of SAI in decreasing extreme precipitation events and consecutive wet days are more pronounced than ~~that of in~~ G6solar. While the ~~results from both~~ G6sulfur and G6solar show encouraging potential abatement of ~~many of the impacts on from~~ detrimental extreme events ~~that which~~ are similar with the lower emissions target of SSP2-

35 ~~4.5, evident in SSP5-8.5~~ there are some exceptions. ~~For instance, Both both~~ G6sulfur and G6solar show drying ~~trends~~ at high latitudes ~~within the regions~~, which is consistent with our understanding of the spin-down of the hydrological cycle under SRM. ~~For instance, the projected dry days increase for G6sulfur compared to SSP5-8.5.~~ These side effects imply that a cautionary approach and further optimization may be required should any future SRM deployment be considered.

1 Introduction

40 China, as a country that hosts the world's second largest population, is acutely vulnerable to extreme hydrological events caused by climate change. For example, climate change can cause sea-level rise which could significantly impact flooding hazards for coastal cities in China, and flooding events in China are consistently ~~predicted-projected~~ to increase under the influence of rising ~~greenhouse gas (GHG) (high level greenhouse gas)~~ emissions. For example, studies show that precipitation ~~and flooding caused by heavy rainfall events~~ will increase across China by the end of the 21st century ~~with previous research~~
45 ~~projecting that heavy rainfall events cause increased flooding in the 21st century (Ying et al., 2014; Yang et al., 2021; Zhnag and Zhou., 2020).~~ ~~In addition to an increase in extreme precipitation, it has also been suggested that the most populated south-eastern China would experience higher flood hazard risks across all future periods (2016-2035, 2046-2065, and 2080-2099) (Ying et al., 2014).~~ Extreme precipitation events appear to have impacted China more often in recent years; ~~For example, in the summer of 2020, the summer of 2020 was anomalous,~~ with ~~severe~~ flooding ~~occurred~~ in southern, eastern, and parts of
50 central China (Jia et al., 2022). In the summer of 2021, unprecedented rainfall hit Zhengzhou, ~~the capital and central city of Henan province, causing severe flooding with a rainfall an~~ intensity of over 200 mm per hour (Zhao et al., 2021) ~~and. The leading cause of the heavy rainfall was Typhoon In fa and continuous subtropical high pressure (Jackson and Shawn, 2021). Strong low level easterly or south easterly jets developed between the western Pacific subtropical high (WPSH) and Typhoon In Fa (Rao et al., 2023) bringing a large amount of moisture from the ocean to Henan Province that caused heavy rainfall~~
55 ~~(Deng et al., 2022). The precipitation further accumulated, exceeding over 550 mm within 24 hours. It has been designated as the '7.20 Henan extreme urban flooding event' (Dong et al., 2022).~~ In 2022, although southern China continued to suffer from extreme precipitation, the flooding ~~was risk has been centred centring to in~~ the west of the Yangtze River, including provinces such as Sichuan and Qinghai which have experienced sudden heavy rainfall events. ~~Although not statistically robust, these events might tentatively suggest a potential expansion of the regions that could be influenced by increasing precipitation in~~
60 ~~China under the changing climate. Commencing on In July 29, of 2023, a record-breaking episode of rainfall and flooding unfolded across at least 16 cities and provinces in north-eastern China. Notably, Beijing encountered the most substantial precipitation event in the past 140 years, with accumulated rainfall exceeding 60% of the region's typical annual precipitation within a remarkably brief span of 83 hours (CDP, 2023). This led to flooding in cities, including Beijing, resulting in at least 60 fatalities and significant damage to homes, crops, livestock, and infrastructure (REUTERS, 2023).~~ ~~Although not statistically~~
65 ~~robust, these events might tentatively suggest a potential expansion of regions that could be influenced by increasing precipitation under the changing climate.~~ On a global scale, climate change ~~appears to have has~~ been influencing hydroclimatic

conditions (Donat et al., 2016; Pendergrass and Knutti, 2018). The direct influence of global warming is that rising atmospheric temperatures induce stronger evapotranspiration and the atmosphere can hold more water vapour. The intensified hydrological cycle exacerbates heavy rainfall and flooding but can also contribute to further drying over land areas and prolonged drought periods (IPCC, 2021). ~~Climate change induced faster evaporation causes and higher atmospheric temperatures induce more moisture laden air in the storm tracks. Consequently, Precipitation tends to increase significantly during events commonly classified as extreme in response to warming (Pendergrass and Knutti, 2018) in general, wet areas become wetter while dry areas become drier (Held and Soden, 2006).~~ Extreme weather events including droughts and flooding could be worsened by global warming. A global-scale study indicates that global warming will potentially increase drought severity as well as drought frequency in the future (Qi et al., 2022). Flooding events also occur at higher frequency and intensity under extreme precipitation amplification (Tabari, 2020). Weather and climate disasters such as extreme temperatures and severe snowstorms, have caused serious economic losses in densely populated East Asian countries (Huang et al., 2007; Li et al., 2016). An increase in precipitation forecasted by current climate models, particularly over the populated areas in East Asia, such as China (Liang and Haywood., 2023) implies strategies are urgently needed to mitigate changes in hydrological extremes.

Owing to the difficulties in achieving climate targets such as the 1.5°C or 2°C above pre-industrial levels proposed by the Paris Conference of Parties (IPCC, 2018), Solar Radiation Modification (SRM) proposals, i.e. strategies to mitigate the worst impacts of climate change by brightening the planet have been studied (Haywood et al., 2022). To understand the robust climate model responses to geoengineering, the Geoengineering Model Intercomparison Project (GeoMIP) was established to provide a comprehensive multi-model assessment of the effects of SRM (Kravitz et al., 2013; Kravitz et al., 2011). ~~Modelling SAI geoengineering (e.g. G6sulfur experiment) is one of the most prominent SRM strategies within the GeoMIP suite of recent simulations (Vioni et al., 2022).- To some extent, SAI can partially counteract climate warming by injecting reflective particles, or their gaseous precursors, into the stratosphere (Zarnetske et al., 2021). In addition to reducing the temperature, SAI also influences tropospheric and stratospheric ozone, terrestrial ecosystem, terrestrial carbon, and hydrological cycle by changing the physical climate system and atmospheric chemistry. Numerous studies support these effects associated with volcanic eruptions and their simulation through SAI techniques (e.g. Imai et al., 2020; Mclandress et al., 2011; Jones et al., 2018, 2020; Liang and Haywood., 2023; Lee et al., 2021; Plazzotta et al., 2019; Vioni et al., 2022).SAI mitigates anthropogenic climate warming by injecting reflective particles, or their gaseous precursors, into the stratosphere. The resultant aerosols reflect and scatter solar radiation back into space leading to a cooling that counterbalances the warming from increased concentrations of greenhouse gases (e.g. Stenchikov et al., 1998). Such simulations mimic the explosive 1991 eruption of Mount Pinatubo in the Philippines; this volcanic eruption created a layer of stratospheric aerosol that induced a cooling of global average surface temperature by around 0.5 degrees Celsius for around two years (Bluth et al., 1992; Self et al., 1996; Robock, 2000). There have been other smaller eruptions since then that have also been modelled to exert a cooling influence, the climate (Soden et al., 2002; Haywood et al., 2014; Schmidt et al., 2018). In addition to reducing the temperature, SAI also influences tropospheric and stratospheric ozone, terrestrial ecosystem, terrestrial carbon, and hydrological cycle by changing~~

100 ~~the physical climate system and atmospheric chemistry (Liang and Haywood., 2023; Jones et al., 2018; Jones et al., 2020; Cao, 2018; Plazzotta et al., 2019; Lee et al., 2021; Visioni et al., 2022; Imai et al., 2020; Melandress et al., 2011).~~

The latest phase of policy-relevant GeoMIP simulations (GeoMIP6) proposed two new experiments, G6sulfur and G6solar (Kravitz et al., 2015), which are designed to simulate the influence of SAI and solar constant reduction to the end of the 21st century based on predicted future emission pathways (Shared Socioeconomic Pathway; SSPs). G6sulfur and G6solar aim to
105 lower global mean surface temperatures from a high-tier emission scenario (SSP5-8.5; ~~(Meinshausen et al., 2020)~~) to a medium-tier emission scenario (SSP2-4.5). These SSP scenarios were developed by the Coupled Model Intercomparison Project Phase 6 (CMIP6; Eyring et al., 2016), which provides multi-model climate ~~predictions~~ projections based on alternative scenarios of future emissions and land use changes produced by integrated assessment models (O'Neill et al., 2016). Studies such as Jones et al. (2021) and Ji et al. (2018) included detailed descriptions and explanations of the CMIP6, GeoMIP, and the
110 differences in models' assumptions. Previous studies indicated SAI would~~will~~ exert a negative radiative forcing and reduce near-surface air temperature (including temperature means and extremes)~~(Pinto et al., 2020)~~, and precipitation (Pinto et al., 2020; Liu et al., 2021). For example, The GLENS experiments revealed significant alterations in precipitation patterns across tropical and midlatitude regions when sulfate geoengineering counteracts global warming (Simpson et al., 2019). However, as suggested by some studies, although SAI can effectively counteract anthropogenic global warming at the global scale, it cannot
115 fully offset the effects at regional scale (Niemeier et al., 2013; Tilmes et al., 2013; Tye et al., 2022). Furthermore, the climate effects in terms of magnitude as well as spatial and temporal distribution depend largely on the scenario of SAI deployment. To date, only a few studies have concentrated on the impact of SAI on the future changes in weather systems over East Asia (Liang and Haywood., 2023; Liu et al., 2023; Tew et al., 2023).

In this study, we focus on~~analyse~~ the potential effects of SAI geoengineering the projected change of precipitation over China in the 21st century, particularly focused on the effects of G6sulfur and G6solar on hydrological extremes over China. , using
120 Based on simulations of the UKESM1 model and CMIP6 experiments~~-. Our our~~ study explores the changes in frequency and intensity of extreme precipitation between the latest future GHG emission scenarios and solar geoengineering (G6sulfur, G6solar)~~scenarios. We focus on~~ The results of the period towards the end of this century, 2070-2100, were compared with that of control period (CP: 1981-2010). to maximize the signal to noise in the simulations as the SAI injection rates increase
125 throughout the century. Section 2 describes the experimental design and details of the model used in this study. In Section 3, results are presented to show the changes in extreme indices in China ~~both~~ under the ~~use of~~ SAI (G6sulfur) and solar constant reduction (G6solar) during 2071-2011, compared to control period present day and climate change future emission scenarios (SSP5-8.5, SSP2-4.5). The regional analysis of China's extreme precipitation and cumulative distribution function is also provided in Section 3. Section 4 summarises and discusses the findings.

2.1 Study area

To quantitatively examine regional differences and better visualize the future extreme climate features, China is divided into 7 different sub-regions (Fig.1) to distinguish extreme climates across the following regions: Northeast China (NEC), North China (NC), Northwest China (NWC), Centre China (CC), East China (EC), South China (SC), and Southwest China (SWC) following Liang et al. (2023).

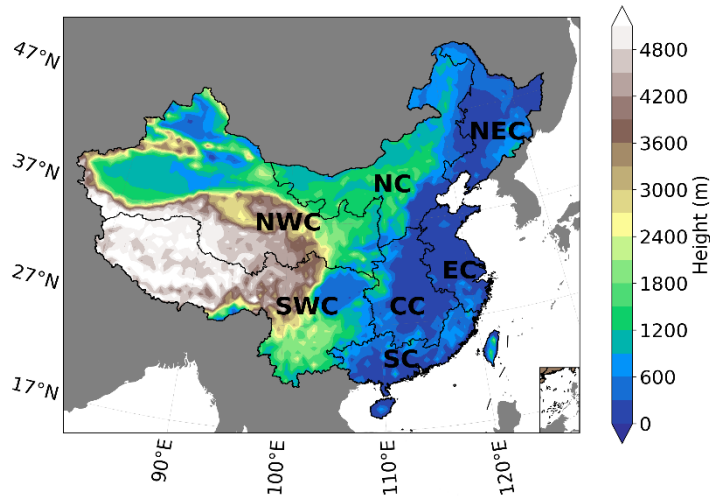


Figure 1: Geological map of elevation and 7 sub-regions in China (unit: m), data from (Liang et al., 2023)

2.2 UKSEM1 model and model simulations

~~In this study was based on the simulations by , data from G6sulfur and G6solar experiments are used from the sixth phase of GeoMIP from~~ the U.K. Earth System Model UKESM1 (Sellar et al., 2019). UKESM1 contains the sophisticated United Kingdom Chemistry and Aerosols (UKCA) module that represents the sulphur cycle in the troposphere and stratosphere (Archibald et al., 2020). ~~UKESM1~~ is a fully coupled ~~Earth system~~ model with ~~an atmospheric~~ resolution of 1.25° latitude by 1.875° longitude (Storkey et al., 2018; Walters et al., 2019; Mulcahy et al., 2018, Sellar et al., 2019), and contributes to both CMIP6 and GeoMIP6 (Jones et al., 2020). The Scenario MIP high GHG forcing scenario SSP5-8.5 (O’neill et al., 2016) is used as the baseline scenario of both G6solar and G6sulfur experiments (Kravitz et al., 2015). ~~The G6sulfur experiment injects SO₂ into the stratosphere to adjust the global mean surface temperature from SSP5-8.5 to that of the SSP2-4.5 medium forcing scenario over the period 2020-2100 (Haywood et al., 2022). The GeoMIP G6sulfur simulations that reduce global mean temperatures from the SSP5-8.5 scenario to the SSP2-4.5 scenario are described in detail elsewhere (Kravitz et al., 2015).~~ In

150 ~~the G6sulfur experiment.~~ UKESM1 simulates SO₂ injection in the stratosphere along the Greenwich meridian at an altitude
of 18-20 km between 10° N and 10° S ~~in G6sulfur~~ (Kravitz et al., 2021; Haywood et al., 2022). ~~UKESM1 contains the
sophisticated United Kingdom Chemistry and Aerosols (UKCA) module that represents the sulphur cycle in the troposphere
and stratosphere (Archibald et al., 2020).~~ A parallel experiment to ~~the~~ G6sulfur, the G6solar experiment, reduces ScenarioMIP
Tier 1 high forcing scenario to the medium forcing scenario by reducing solar irradiance. ~~Reductions in the global mean near-
surface temperature, from those of SSP5-8.5 to those of SSP2-4.5 are achieved by reducing the solar constant or increasing
SAI by trial and error to within a tolerance of ±0.2 K (Visioni et al., 2021).~~ Notably, it is anticipated that the G6solar will
155 exhibit reduced inter-model disparities in the spatial distribution of forcing when compared to the G6sulfur owing to model
differences in representing the complexities of the sulfur cycle within global models. Therefore, the G6solar is proposed as a
parallel experiment to the G6sulfur for the purpose of comparing the impacts of solar reduction with those of stratospheric
aerosols. (Kravitz et al., 2015).

160 In the UKESM1 model, three ensemble members, ‘r1ilp1f2’, ‘r4ilp1f2’, and ‘r8ilp1f2’, are run for the G6sulfur and the
G6solar as specified in the GeoMIP protocol (Kravitz et al., 2015). We calculated the ensemble mean for all simulations,
including SSP5-8.5, SSP2-4.5, G6sulfur, G6solar and Historical. The future changes in extreme climates were assessed by
comparing the future simulations (SSP5-8.5, SSP2-4.5, G6sulfur, G6solar) for the period 2071-2100 with the ~~present-
day control~~ period 1981-2010 ~~(Historical)~~, using the UKESM1 historical simulations for CMIP6. The results for the ~~future final~~
165 30 years of the 21st century (2071-2100) from the simulations were used to investigate the influences of the G6sulfur and the
G6solar experiments. ~~The rationale for using the present day period as a baseline for comparison is that the model performance
for the present day can be assessed against observed climate metrics to provide guidance of model fidelity as described in the
following subsections.~~

2.3 Aphrodite precipitation data

170 The APHRODITE (Asian Precipitation-Highly-Resolved Observational Data Integration Towards Evaluation) was
interpolated from gauge-observation data with a resolution of 0.25°× 0.25° (Lai et al., 2020; Yatagai et al., 2012), and were
used to validate the performance of the UKESM1 model in simulating ~~present day the control period~~ extremes. APHRODITE
~~is has been~~ a dataset containing long-term gridded daily precipitation (1951-2015). The high-resolution daily product of
APHRODITE is developed based on the rain-gauge data across Asia presented on a continental scale (Sunilkumar et al., 2019).
175 In this study, we ~~apply applied the~~ APHRODITE’s climatological daily mean precipitation as observation data ~~for and~~
validatinge the UKESM1 ~~historical~~ simulations.

2.4 Extremes precipitation indices

180 ~~To quantify extreme precipitation, a range of indices were defined by The results were assessed according to the IPCC World Climate Research Programme (WCRP) defined extreme precipitation indices to quantify the precipitation extreme responses in each experiment. In this study, We selected eight extreme indices were selected according to defined by the WCRP's Expert Team on Climate Change Detection and Indices (ETCCDI), as shown in Table 1 to perform the analysis on all of the simulations.~~

Table 1: The definition of selected extreme indices based on ETCCDI (Firsch et al, 2002; Klein Tank et al., 2002, 2009)

Indices	Descriptive name	Definition	Units
DD	Dry days	Count of days when precipitation < 1 mm	days
CDD	Consecutive dry days	Maximum number of consecutive days with < 1 mm of precipitation	days
CWD	Consecutive wet days	Maximum number of consecutive days with ≥ 1 mm of precipitation	days
R50MM	Rainstorm days	Count of days when precipitation ≥ 50 mm	days
RX1DAY	Maximum 1-day precipitation	Annual maximum 1-day precipitation	mm
RX5DAY	Maximum 5-day precipitation	Annual maximum <u>consecutive</u> 5-day precipitation	mm
R95p	Very wet days	Annual precipitation amount accumulated on days when daily precipitation is greater than the 95th percentile threshold of the wet-day precipitation	mm

185

2.5 Statistical methods and Cumulative Distribution Functions (CDFs)

~~In the validation section comparing the experiment's ensemble mean with observed Aphrodite data, At first, for validating the model simulations, the Aphrodite data was re-gridded to the resolution of the UKESM1 ensemble mean data. the ensemble mean was re-gridded to the resolution of the Aphrodite data after averaging. This study simulates the changes in precipitation~~

190 ~~between different experiments in terms of annual mean differences.~~ To examine the statistical importance of the ~~results changes~~
~~in precipitation between different experiments,~~ we performed the Wilcoxon Rank Sum Test ~~instead of the more commonly~~
~~used Student's t test.~~ Wilcoxon Rank Sum Tests works as a non-parametric two-sample t-test and is more appropriate for use
with atmospheric data (Wilks, 2011), with ~~a 5% confidence level of p-value < 0.05 suggesting~~ statistical significance.

To better visualize the future extreme climate features and the effects of SAI, the Cumulative Distribution Functions (CDFs)
195 for rainfall have been calculated. CDFs is frequently employed for bias correction to enhance the accuracy of rainfall analysis
(e.g., Apurv et al., 2015; Rana et al., 2014; Xiong et al., 2019). ~~This decision accounts for the mixed nature of our data, as~~
~~extreme precipitation can be viewed from both continuous and discrete perspectives. While Probability Density Functions~~
~~(PDFs) are conventionally used for continuous variables (Vidhya, 2023), our focus on annual extreme precipitation, often~~
~~treated as discrete events, aligns well with the suitability of CDFs.~~ This approach allows for a nuanced exploration of the
200 distribution, accommodating the continuous and discrete aspects of our dataset. The calculated CDFs offer a holistic
perspective, providing insights into the probability distribution patterns for various events over the study period.

Unlike Tung et al. (2022), where CDFs were employed, a choice was made to use reversed CDFs in our study to better illustrate
the thresholds for rainfall events exceeding certain values. To achieve this, during the continuous 30-year study period, we
computed the average annual extreme precipitation index values for each grid point and plotted their CDFs over all grid points
205 in a region. This analysis facilitated the observation of continuous probability distribution patterns and the assessment of tail-
end magnitudes, providing insights into the continuous likelihood of varying precipitation levels and revealing extremes
throughout the studied period.

3. Results

In order to comprehensively assess the statistical significance of our findings, a 'field significance' analysis based on the method
210 proposed by Wilks (2006) was employed. This approach allows us to evaluate the significance in regions without observed
data points. The calculations were conducted using the following Eq. (1):

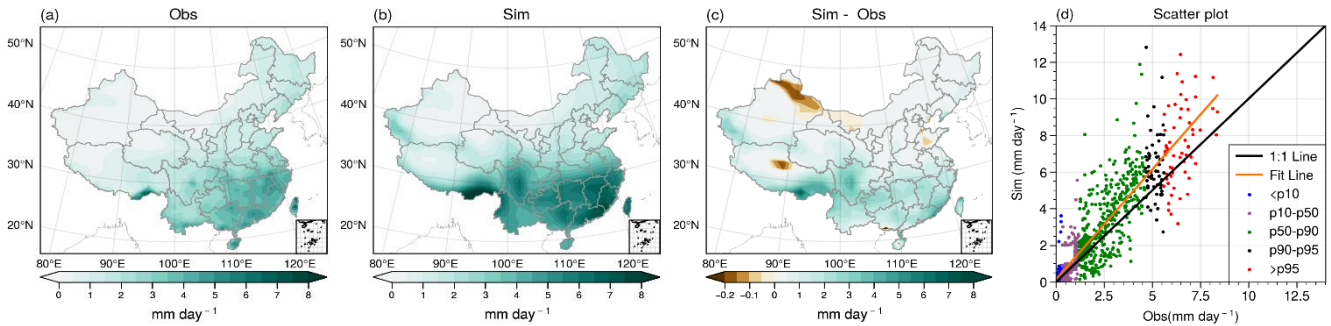
$$\Pr(M \geq m) = \sum_{i=m}^K \frac{K!}{i!(K-i)!} \cdot (\alpha_{local})^i \cdot (1 - \alpha_{local})^{K-i} \quad (1)$$

215 where 'm' represents the number of observed data points identified as statistically significant through significance testing, 'K'
is the total number of grid points, and ' α_{local} ' is the local significance level.

According to the calculation using this formula, all non-dotted regions exhibit statistical significance. However, detailed
explanations of this process are omitted for brevity in this paper.

3.1. Precipitation changes

- 220 Figure 2 shows the spatial distribution pattern of observed and simulated mean precipitation over China bias between simulated present-day during the control period (PDCP; mean of 1981-2010) and comparisons between the two datasets data and observed Aphrodite data of 30 years is shown in Fig.2. The PD data is derived from the UKESM1 historical simulations. Evaluation of annual mean land precipitation simulations of UKESM1 model (PD) (Fig.2b) against observed data (Obs) (Fig.2a) reveals that, while the general pattern of the simulated precipitation (Fig.2b) was similar to the observed precipitation (Fig.2a) accurate,
- 225 the amount of precipitation simulated tends to be somewhat larger than the observed over much of China, as indicated in Fig.2c. Both results show a general decreasing trend from the southeast coastal regions to the northwest inland areas is well simulated. The wet bias in daily precipitation is evident in most parts of southern China (SC, CC, and SWC), particularly on the south-eastern flanks of the Qinghai-Tibet Plateau (QTP). Regions with dry bias are relatively small (shown by the negative values and brown contours in Fig.2c), with bias values less than 1 mm day⁻¹.
- 230 To further compare the results between simulations and observations, particularly focusing on extreme precipitation values, a scatter plot between the ensemble mean simulations and observations is provided as Fig.2d (the scatter plots comparing the simulations of the three model ensembles with the observations are provided in Fig.S1). For the purpose to evaluate the model performance at different level of precipitation, the daily precipitation was as classified in to several intervals: P10 (the smallest 10%), P10-50, P50-90, P90-95, and P95 (the largest 5%). In order to indicate the bias as a percent, relative changes (compared
- 235 to the observations) for different intervals have been calculated, as listed in Table 2.



- 240 Figure 2. Spatial distributions of mean land precipitation (units: mm day⁻¹) over China during the control period of 1981-2010 for (a) the observations (Obs), (b) the simulations (Sim), (c) the bias (Sim-Obs), and (d) a scatter plot between the observations and simulations at different level of precipitation.

Figure 2. Spatial distributions of mean land precipitation (units: mm day⁻¹) over China during the period of 1981-2010 from (a) Obs (observed Aphrodite data), (b) PD data (simulated multi-ensembles historical data), (c) the bias between

~~PD and observed, and (d) scatter plots between the observations and model results at different level of precipitation during the CP.~~

Table 2: Relative changes of the model results (compared to the observations)

<u>intervals</u>	<u>Ensemble mean</u>	<u>r1i1p1f2</u>	<u>r4 i1p1f2</u>	<u>r8i1p1f2</u>
<u><P10</u>	<u>89.81%</u>	<u>93.95%</u>	<u>89.44%</u>	<u>86.04%</u>
<u>P10-50</u>	<u>30.05%</u>	<u>30.38%</u>	<u>31.85%</u>	<u>27.13%</u>
<u>P50-90</u>	<u>30.50%</u>	<u>28.95%</u>	<u>31.36%</u>	<u>31.16%</u>
<u>P90-95</u>	<u>24.03%</u>	<u>22.79%</u>	<u>24.85%</u>	<u>24.44%</u>
<u>>P95</u>	<u>15.76%</u>	<u>15.09%</u>	<u>16.27%</u>	<u>15.92%</u>

The scatter plots (Fig.2d and Fig.S1) indicate a close relationship between the observations and the simulations. However, the simulations are generally higher than observations, possibly because of the different resolution of the data. Since our study has been mainly focused on the relative changes between the future results and that of control period for different scenarios, the systematic bias would not affect the conclusions significantly. As expected, relative changes are very large at small values (below the 10th percentile), both for the ensemble mean and the model members. For the results at the 10-50th and 50-90th percentiles, relative changes are around 30%. When larger than the 95th percentile, relative changes are relatively small, near 15%. The differences among ensemble members are not significant, which suggests the uncertainty in the ensembled results is reasonable and acceptable.

Figure 3 illustrates the spatial distribution of relative changes in mean precipitation—changes in ‘mm/day’ units over land areas for different simulations during the future period 2071-2100 compared with relative to the control period PDCP for UKESM1. In all the four simulations, most part of the region is dominated by increased precipitation as captured by all the experiments. For SSP5-8.5 (Fig.3a), the most prominent increase in precipitation occurs within SC, but the precipitation in SC, northern Taiwan and Hainan is projected to decrease in the future. SSP2-4.5 (Fig.3b), similar patterns can be seen are noted under SSP2-4.5 (Fig.3b) while but the magnitude of increases in precipitation is generally reduced, particularly in SC, by about 50% relative to SSP5-8.5. For G6sulfur (Fig.3c), changes are similar to that of SSP2-4.5, indicating the SAI is approximately successful. Both G6sulfur (Fig.3c) and G6solar (Fig.3d) (SRM) show ameliorated change with respect to SSP5-8.5, meaning that the SRM mitigate the increase in precipitation in China that occurs in SSP5-8.5.

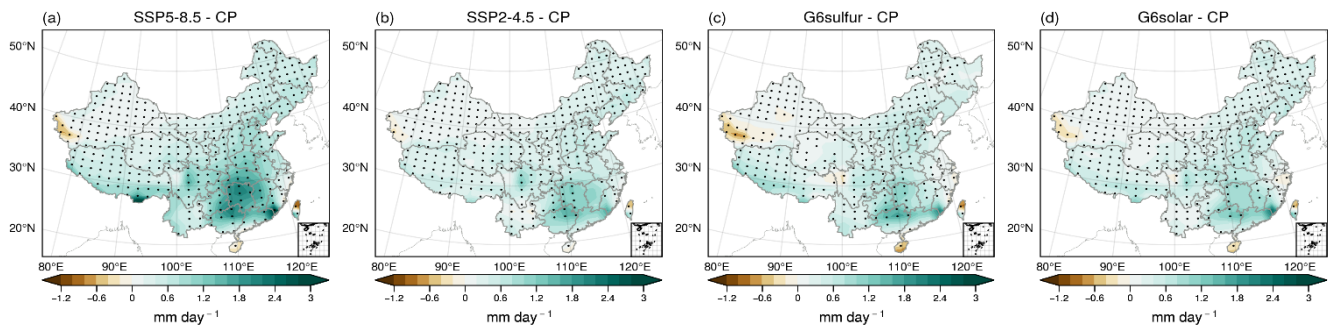


Figure 3. Relative changes in land precipitation (mm day^{-1}) of the period 2071-2100 compared to that of the **PD (1981-2010) (a) SSP5-8.5, (b) SSP2-4.5, (c) G6sulfur, and (d) G6solar. ~~The PD data comprise years 1981-2010 from the UKESM1 historical simulations.~~ The dotted areas indicate where the difference is statistically significant at 95% confidence level using a Wilcoxon rank sum test.**

Figure S2 compares the simulated future precipitation between G6sulfur and other experiments. Compared with SSP5-8.5 (Fig. S2(a)), the simulated SAI by G6sulfur leads to a decrease in precipitation over almost the entire China. ~~This suggests that the effect of SAI on future precipitation is more widespread and remarkable compared to that of SSP5-8.5~~ ~~This suggests that SAI is sensitive to global warming in China~~, particularly over the SWC (southeast QTP) and CC regions. The difference in precipitation between G6sulfur and SSP2-4.5 (Fig. S2(b))/G6solar (Fig. S2(c)) is smaller compared to the difference between G6sulfur and SSP5-8.5 (Fig. S2(a)). This indicates SAI effectively mitigates the increase in mean precipitation from the high GHG SSP5-8.5 scenario to the medium GHG SSP2-4.5 scenario across most of China.

3.2. Hydrological extreme changes

~~In this section, we examine impacts on hydrological extreme indices changes by presenting geographic maps of the chosen variables. As extreme rainfall events are associated with the tail of the CDFs, the tails of the CDFs have been focused on by adjusting the vertical axis to range from 0% to 10%, and the Aphrodite data has been excluded for clarity.~~

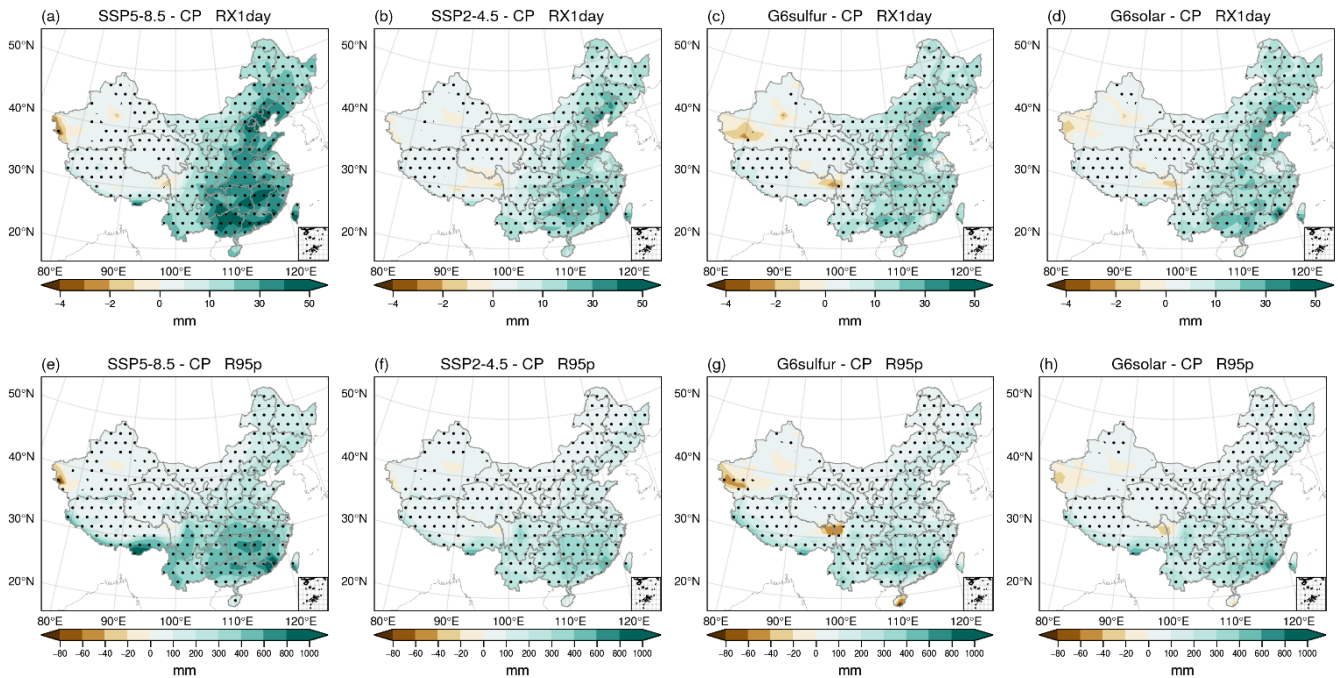
3.2.1 Wet extreme changes

The small-scale flooding risk is ~~now being~~ assessed by the RX1day index, and the extreme threshold index of very wet day precipitation ~~is represented by the R95p is being used~~, ~~for which the 95th percentile of threshold was computed for each grid based on the 30 years (1981-2010) daily precipitation.~~ The changes in RX1day and R95p for the future period (2071-2100) relative to the ~~historical baseline control~~ period (1981-2010) are shown in Fig.4. Simulations under the SSP5-8.5 scenario project significant increases ($p\text{-value} < 0.05$) in RX1day in east China (Fig.4a). The greatest magnitude of increase (above 50

mm) is seen in SC, CC, east coastal NC and a small part of SWC regions. Under SSP2-4.5 (Fig.4b), a similar pattern of the
290 RX1day change to SSP5-8.5 is projected but with smaller magnitudes. G6sulfur (Fig.4c) and G6solar (Fig.4d) show generally
ameliorated changes compared to SSP5-8.5.

In the future, an increase in RX5day is anticipated across most of China, with the most substantial increments occurring in the
eastern part of the country and on the QTP (Fig. ~~S2AS3a-d~~). The largest increases are anticipated under the SSP2-8.5 scenario
(Fig.~~S2AS3a~~), reaching a maximum of over 100 mm. In the other three G6 ~~models~~scenarios, ~~the increase in RX5day is~~
295 ~~considerably smaller than that under SSP5-8.5, with none exceeding 100 mm compared to the control period (Fig.S3a-d)~~~~the~~
~~rise in RX5day is considerably smaller under SSP5-8.5, with none exceeding 100 mm.~~ This suggests a mitigated future RX5day
simulation compared to SSP5-8.5 in these three models. It is noteworthy that under G6solar (Fig.~~S2DS3d~~), the maximum
RX5day is observed in the south-eastern part of the SC region.

R95p is projected to significantly increase ~~(p-value < 0.05)~~ in CC, SC, and south SWC regions under SSP5-8.5 scenario
300 (Fig.4e), ~~which is generally~~ consistent with a previous study (Wang et al., 2016; ~~Qin and Xie., 2016; Peng et al., 2018~~). This
increase has been attributed to the strengthened south-westerly winds across south China caused by the land-sea contrast
between China and adjacent oceans. Furthermore, global warming also contributes to the increased water vapor, thereby
enhancing the likelihood of precipitation and related extremes (Tang et al., 2021). The SSP2-4.5, G6sulfur and G6solar
experiments present similar spatial distributions, but smaller magnitudes of changes (Fig.4f-h). G6sulfur (Fig.4g) shows a
305 significant decrease in highly populated areas of Hainan (south SC) compared to SSP5-8.5. ~~This suggests that SAI SRM~~
~~appears to effectively mitigate the R95p increase relative to the high SSP5-8.5 scenario in this area, although we caution over~~
~~interpretation of this result over such a small geographical area.~~

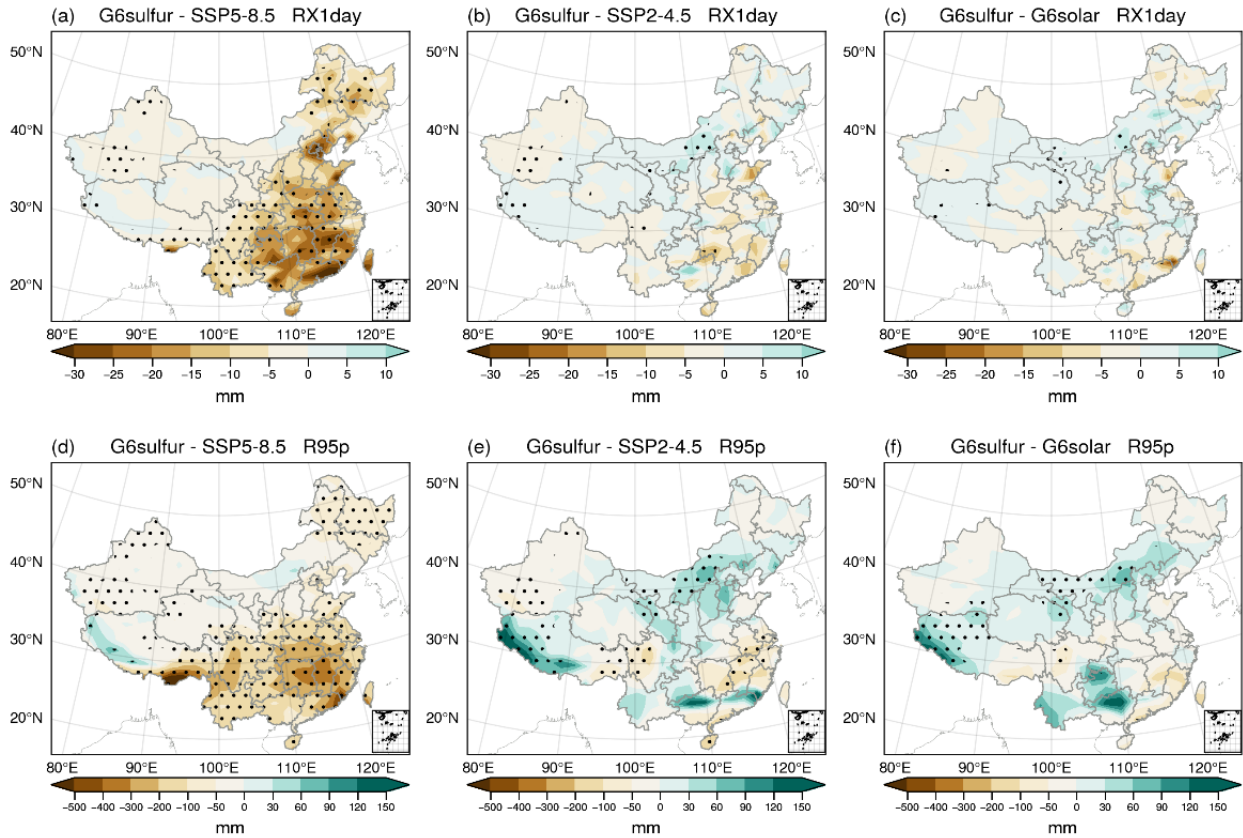


310 **Figure 4. Relative changes in RX1day (a-d) and R95p (e-h) for the future period of 2071 – 2100 compared to the control**
period PD(CP). The dotted areas indicate where the difference is statistically significant at 95% confidence level using
a Wilcoxon rank sum test.

315 Figure 5 illustrates how SAI modulates the distribution of extreme precipitation intensity indices by ~~dieipting~~ depicting
~~The comparisons confirm that G6sulfur can effectively ameliorate the~~
~~increase in the intensity indices in eastern China (shown by the negative brown shaded areas in Fig.5 a and d).~~ A previous
study demonstrated that the reduction of emissions of anthropogenic aerosols is a key factor leading to increased extreme
intensity indices over most of China by the end of 21st century (Wang et al., 2016). Compared with SSP2-4.5 (Fig.5b) and
320 G6solar (Fig.5c), G6sulfur leads to only small changes of less than 20mm in RX1day. The similarity of G6sulfur to SSP2-4.5
and G6solar suggests that the primary impact on RX1day over China is driven simply by the temperature; a global mean
temperature of the standard CMIP6 SSP2-4.5 scenario gives very similar results to those achieved when SSP5-8.5
temperatures are brought down to those of SSP2-4.5. However, the same cannot be said for R95p, where the ensemble mean of UKESMI
projects a significant increase in SC and southwestern SWC (Fig.5e) for the G6sulfur (2071-2100) relative to the SSP2-4.5
(2071-2100), and in north SC, eastern, and southwestern SWC relative to G6solar (Fig.5f).

325 From Figure S3AS4a, it is evident that G6sulfur effectively mitigates RX5day under SSP5-8.5, particularly in the eastern and
south-western regions. The most notable impact is observed in the SC region and the south QTP, with a mitigation of up to

80mm. ~~This suggests that G6sulfur can efficiently mitigate future flood risks in these areas.~~ In comparison to SSP2-4.5 (Fig.S3B54b), G6sulfur exhibits an increase in RX5day, primarily in the region between 100°E and 120°E. ~~This implies that SSP2 4.5 performs better than G6sulfur in these areas compared to the mitigation effect under SSP5 8.5.~~ For 'G6sulfur-
 330 G6solar' (Fig.S3CS4c), positive values of RX5day are more pronounced in certain areas between 100°E and 120°E, especially in the low latitude zone between 20°N and 30°N. ~~This indicates that G6solar achieves the most effective mitigation of RX5day under SSP5 8.5.~~



335

Figure 5. Differences in RX1Day (a-c) and R95p (d-f) for the future period of 2071 – 2100 between G6sulfur and SSP5-8.5 (a, d), SSP2-4.5 (b, e), and G6solar (c, f). The dotted areas indicate where the difference is statistically significant at a 95% confidence level using a Wilcoxon rank sum test.

340

~~To better illustrate the ameliorating impact of SAI on extreme precipitation under the SSP5 8.5 scenario, the differences between the maximum values of each index under G6sulfur and the SSP5 8.5 scenario, compared to the maximum values~~

under the PD, were aggregated. This process aims to emphasize the mitigation effect of SAI on extreme high values of each index under the SSP5-8.5 scenario. As outlined in Table 2, Table 3 presents the differences in maximum values of the index between the G6sulfur and SSP5-8.5 scenarios. A positive values difference suggests a ~~indicate~~ mitigation effect of SAI, while a negative values signify the ~~opposite~~ difference indicates exacerbation in index thresholds for projected increase regions. In regions where the projected index is decreasing, the meaning of positive and negative signs is opposite to that in regions where the index is projected to increase. In addition, the 0 values indicate there is almost no difference between the maximum index values under G6sulfur and SSP5-8.5, suggesting negligible impact of SAI on indices threshold. G6solar's ameliorating impact in indices thresholds under the SSP5-8.5 scenario has been presented in Supplement Table S1.

Table 23: Amelioration effect of G6sulfur compared to SSP5-8.5 in indices threshold.

	China	NEC	NC	NWC	EC	CC	SC	SWC
RX1day	+	+	+	+	+	+	+	+
RX5day	+	+	+	+	+	+	+	+
R50mm	+	0	+	0	+	+	+	+
CWD	-	-	+	+	-	-	-	-
R95p	+	+	+	+	+	+	+	+
DD	-	-	-	-	-	-	+	-
CDD	-	-	-	-	-	-	+	+

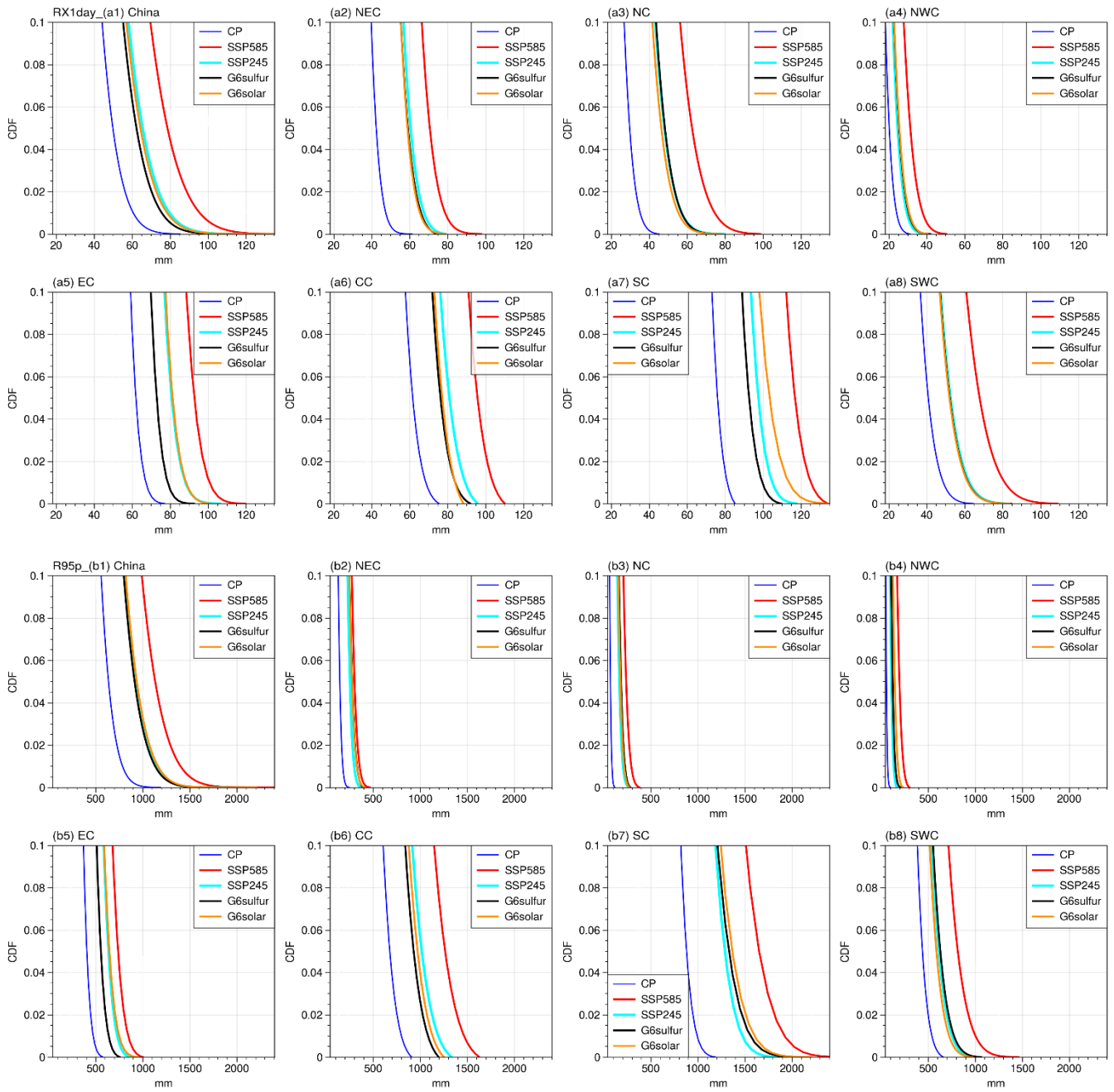
RX1day (Fig.6a) and R95p (Fig.6b) show consistent increases in the future relative to ~~PD~~control period (the blue line). For RX1day the CDFs for precipitation SSP5-8.5 surpasses those from all other scenarios as might be expected from the spatial analyses presented in Fig.4. Additionally, southeastern China (EC, CC, and SC) shows higher values than the northern and western inland regions (NEC, NC, NWC).

The tail of the RX1day CDFs in experiment G6sulfur (black) is close to that of the SSP2-4.5 scenario (cyan) in NEC, NC, NWC, and SWC (Fig.6). Combined with the small and evenly distributed magnitudes shown in Fig.5b, this shows that G6sulfur effectively mitigates SSP5-8.5 to similar the SSP2-4.5 in these regions. In EC, SC and CC, the RX1day CDFs is reduced from that of SSP2-4.5 by between 5-10mm and moves further away from the values seen in the high-end SSP5-8.5 scenarios towards those seen in the ~~historical~~control period simulations. The RX1day CDFs for G6solar are indistinguishable from those for SSP2-4.5 in many regions, but for CC the RX1day lies to the left of the SSP2-4.5 curve but by not as far as that for G6sulfur indicating less abatement of RX1day extremes. Interestingly, for SC, the G6solar CDFs curve lies to the ~~right-left~~ of the ~~SSP2~~SSP5-4.5 curve. Combining the negative value for the SC region in Table ~~S2-S1~~ reveals that the ~~maximum value of~~

365 ~~RX1day under G6solar distribution is even further from that of the PDcontrol period compared to SSP5-8.5, suggesting that while G6solar mitigate the overall RX1day, it exacerbates the maximum RX1day values beyond SSP5-8.5does not mitigate the extreme maximum value of the RX1day index in the SC region.~~

The tail of RX5day CDFs across all regions suggests a future increase in RX5day under four G6 scenarios, with a more pronounced rise under the high SSP5-8.5 scenario. This phenomenon is consistent with the spatial distribution change observed in Fig.4(a-d). In the NEC and CC regions, G6sulfur closely aligns with the SSP2-4.5 scenario (Fig. S4S5). Additionally, in the NC region, G6solar closely mirrors the conditions of the SSP2-4.5 scenario. Combined with the differences in RX5day of spatial distribution in Fig.5, it is evident that G6sulfur mitigates RX5day, resembling the SSP2-4.5 scenario, in NEC and CC regions. Simultaneously, G6solar alleviates RX5day in the NC region, resembling the conditions of the SSP2-4.5 scenario.

375 For R95p, the CDFs of G6sulfur and SSP2-4.5 show no apparent differences for SC, SWC and NWC; however, in EC and CC, there are ~~substantial~~ decreases of more than 100mm, whereas in NEC and NC, there are some increases, ~~although the values only reach about 50mm. It should be stressed here that the regions that are chosen for aggregation are somewhat arbitrary and the results could well change should smaller sub regions be chosen for analysis.~~ For example for the SWC region, Figure 5e reveals that R95p for G6sulfur-SSP2-4.5 shows statistically significant negative values centred at around 30°N 100°E, and statistically significant positive values west of 90°E. Because these regions are aggregated together in the SWC region, there is not a discernible influence on the CDFs of R95p. ~~Thus, the spatial maps and the CDFs should be used in combination when presenting quantitative results.~~



385 **Figure 6. Cumulative distribution functions of RX1day (a1-a8) and R95p (b1-b8) in China and 7 subregions for different scenarios. The same processing was applied to all CDFs figures, including the current one, to enhance clarity: image enlargement, vertical axis adjustment (0% to 10%), and exclusion of Aphrodite data.**

In summary, by the late 21st century, eastern China is projected to experience an increase in heavy rain events and a heightened risk of flooding under the high-emission SSP5-8.5 scenario, with UKESM1 simulations indicating a strengthening of both RX1day and R95p, signaling more stronger precipitation events driven by elevated GHG emissions. ~~Under the G6 scenario, The SRM results are encouraging, showing a reduction in the detrimental extreme events, similar to the lower emissions target of SSP2-4.5. SRM effectively mitigates the increase of RX1day, RX5day and R95p compared to SSP5-8.5 scenario in all regions,~~ particularly in east China and QTP region.

The frequency extreme index change in CWD has been calculated and shown in Fig.7. For the SSP5-8.5 scenario (2071-2100) relative to the ~~PD control period~~ (1981-2010), the ensemble mean of UKESMI predicts a significant decrease (~~p value < 0.05~~) in southwest China (Fig.7a), particularly in the south SWC (QTP), with up to 30-day reduction. This reduction could be influenced by the East Asian and South Asian monsoons under the complex terrain of QTP (Wang et al., 2018). ~~Although CWD is projected to decrease under SSP5-8.5, precipitation amounts increase (Fig.3), suggesting that~~The daily extreme precipitation intensity may rise in southern areas China in the future (Zhu et al., 2018). The increased CWD occurs in mid-latitudes (mostly north of 30°N latitudes) but with a lesser extent (less than 20 days). A similar pattern of change is seen under SSP2-4.5, but with smaller magnitudes (Fig.7b). The experiments G6sulfur (Fig.7c) and G6solar (Fig.7d) exhibit generally mitigated changes compared to SSP5-8.5, although the brown areas shown in Fig.7c are larger than in Fig.7a in NWC.

~~The R50mm index is derived from the Rnmm index, as suggested by ETCCDI. The Rnmm index represents the count of precipitation above a user-chosen threshold. In this case, the threshold is set to 50 mm, as recommended. The absolute threshold rainstorm index, R50mm, is defined as recommended by ETCCDI, with a threshold set to daily precipitation of 50 mm~~ by the China Meteorological Administration (CMA) (Sui et al., 2018). Under the SSP5-8.5 scenario (2071-2100) relative to the ~~PD control period~~ (1981-2010), the ensemble mean of UKESMI projects a significant increase (~~p value < 0.05~~) in populous southern and eastern China (Fig.7e). This aligns with a prior study by Meng et al. (2021), which predicts an increase in R50mm in the lower reaches of the Yangtze River basin and the coastal areas in SC (Meng et al., 2021), indicating a rise in rainstorm events in these regions by the end of the 21st century. This increase in rainstorm events contributes to an elevation in precipitation levels (as shown in Fig.3), exerting significant pressure on social economies and terrestrial ecosystems (as discussed by Peng et al., 2018). A similar pattern of change is observed under SSP2-4.5 (Fig.8f) and in the experiments G6sulfur (Fig.8g) and G6solar (Fig.8h), albeit with smaller magnitudes.

415

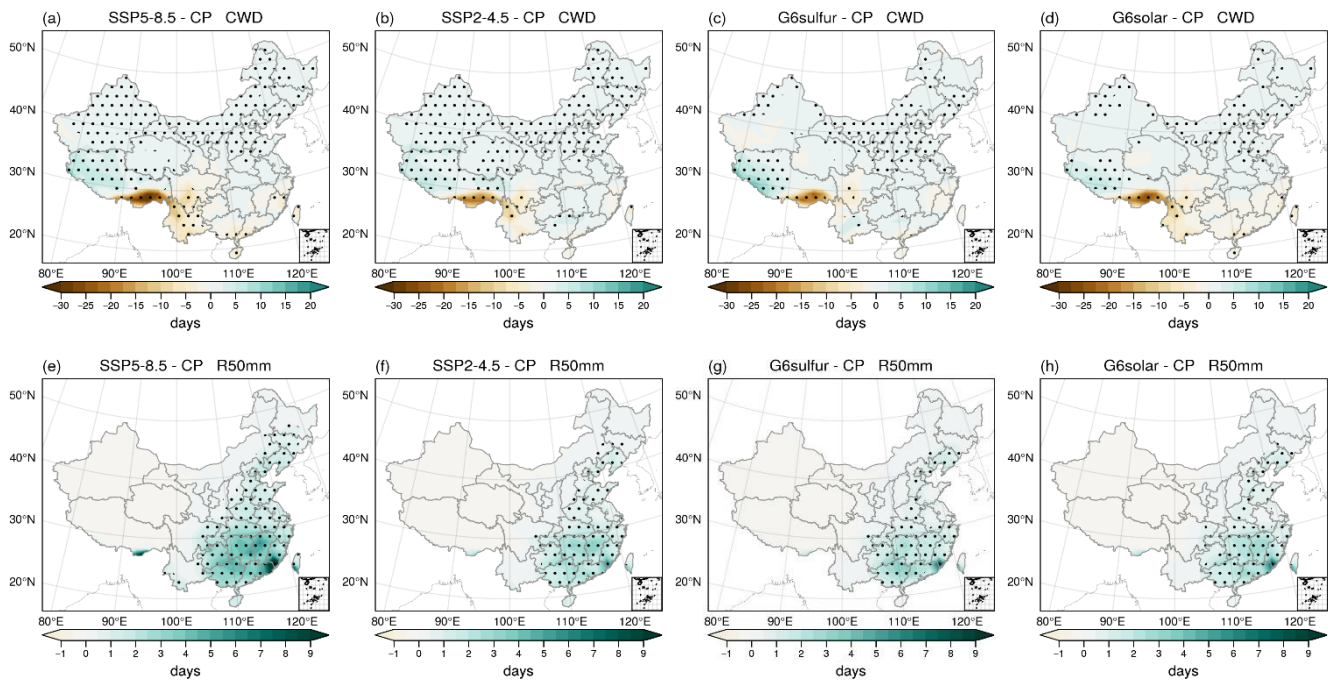


Figure 7. Same as Figure 4, but for CWD (a-d) and R50mm (e-h).

420 Compared to SSP5-8.5 (Fig.8a), G6sulfur significantly increases the CWD in south SWC (by up to 12 days), indicating sensitivity to globe warming within this region. Combined with Fig.7, G6sulfur ~~effectively ameliorates the~~ decrease in CWD under SSP5-8.5 in southeast QTP (approximately 90°E - 100°E). However, in southwest QTP and south China, G6sulfur exacerbates the increase in CWD compared to ~~high-SSP5-8.5-scenario~~, possibly linked to the weakening of the high-altitude westerly jet (driven by the reduced meridional thermal gradient under SAI) that induce an anomalous cyclonic flow dominating

425 QTP (Liang and Haywood, 2023) as per the four-quadrant strait jet model (Uccellini and Johnson, 1979), which creates a precipitation-favouring environments due to the complex terrain and varying altitude in QTP, linked to the cooling effect of concentrated scattering aerosols across lower latitudes. G6sulfur primarily ameliorates the increase in CWD in mid-latitudes (north of 30°N). G6solar (Fig.8c) shows a similar magnitude in south CC and north SC as Fig.8a, suggesting that solar constant reduction does not have a significant effect in CWD compared to SSP5-8.5. For rainstorm (R50mm), G6sulfur leads to a

430 decrease in most part of China, with a significant decrease in south-eastern coastal areas and south QTP, up to 6 days compared to SSP5-8.5. Compared to SSP2-4.5 and G6solar, the differences are close to zero, suggesting that SRM yields nearly identical results to the SSP2-4.5 scenario. ~~In all, SRM effectively ameliorates R50mm under SSP5-8.5 and provides statistically similar outcomes to SSP2-4.5 in China by the end of the 21st century.~~

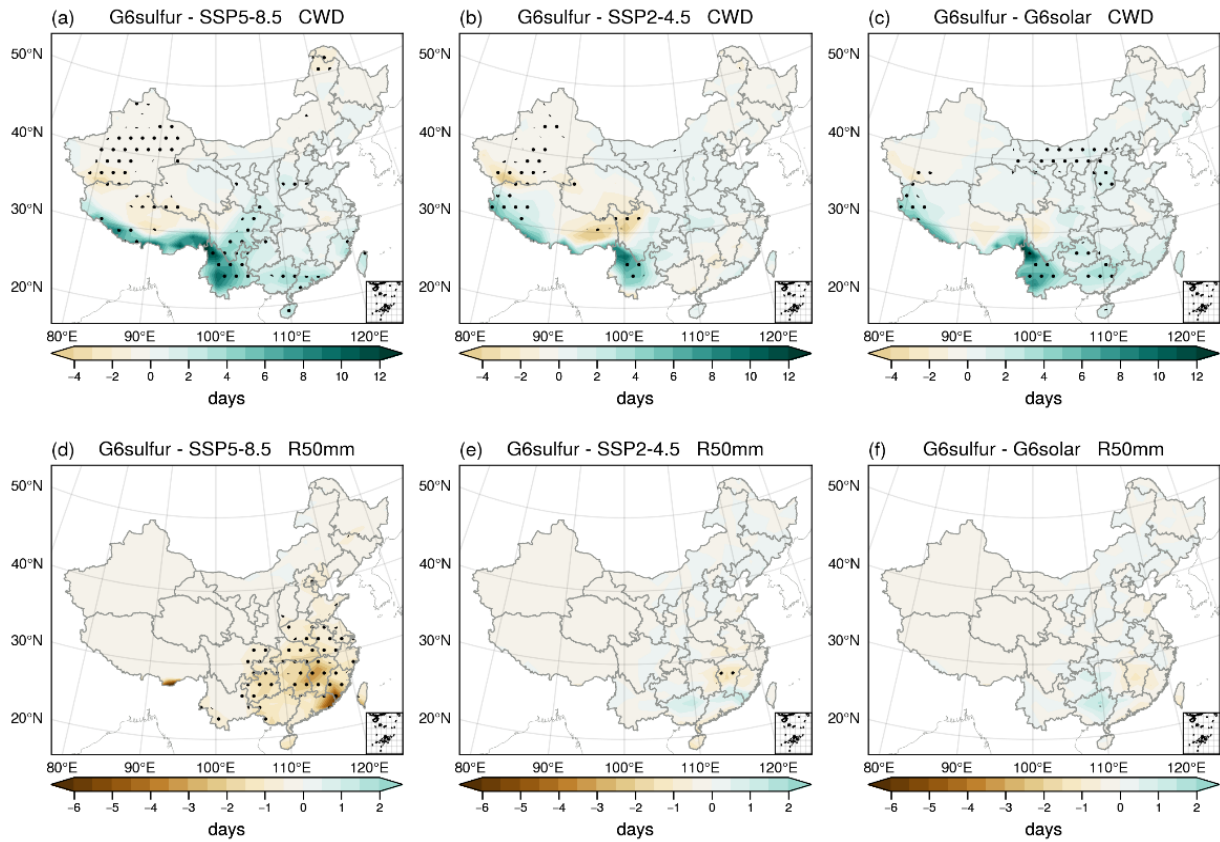


Figure 8. Same as Figure 5, but for CWD (a-c) and R50mm (d-f).

440 The maximum value of CWD in SWC exceeds 200 days, as shown in Fig.9, contributing to a general increase across China (Fig9(a1)). Meanwhile, CWD are projected to decrease, especially in SWC in Fig.9(a8)) and corresponds to the brown shaded areas in SWC as depicted in Fig.7(a-d). In the regions projected to experience an increase of CWD in NE and NWC, the positive value (in Table 3) indicates that SAI experiments produce results of threshold that are closer to the CP conditions. However, the relative effect is not obvious due to the small magnitude of CWD in these regions. The changes in CWD in the future are uncertain, as is whether they increase or decrease relative to PD. Furthermore, CWD under SSP5-8.5 and SSP2-4.5 scenarios does not consistently exhibit simultaneously increases or decreases across all regions. It is notable that in NC, and SC, G6sulfur (black) provides similar results to the SSP2-4.5. When combined with Fig.8b and c (less than 2 days), suggests that G6sulfur yields statistically similar outcome to that of SSP2-4.5 in NC and SC. In SWC, the black line and orange line also closely tracks the cyan line, indicating a similar cumulative distribution of CWD between G6sulfur and SSP2-4.5, and between G6solar and SSP2-4.5. However, there is an uneven spatial distribution, as seen in Fig.8b, and Fig.S5. Consequently, SRM is not expected to reach the levels of SSP2-4.5 in SWC. Interestingly, for EC, SSP2-4.5 yields almost identical statistics

445

450

to SSP5-8.5, while both G6sulfur and G6solar show an increase compared to SSP scenarios. However, the negative values of CWD in EC in Table 2 and S23 indicate that SRM strategies cannot ameliorate the high values of CWD in the EC region. Figure 8(d-f) highlights subtle differences between SSP2-4.5 and SRM strategies a pattern also evident in the CDF analyses illustrating response comparisons. Considering the small magnitude of projected changes and the relatively minor differences in changes between G6sulfur and the other three simulations, coupled with the statistical significance observed in only a few areas in the eastern part. Therefore, moving forward, discussions regarding the CDFs of R50mm will be omitted.

455

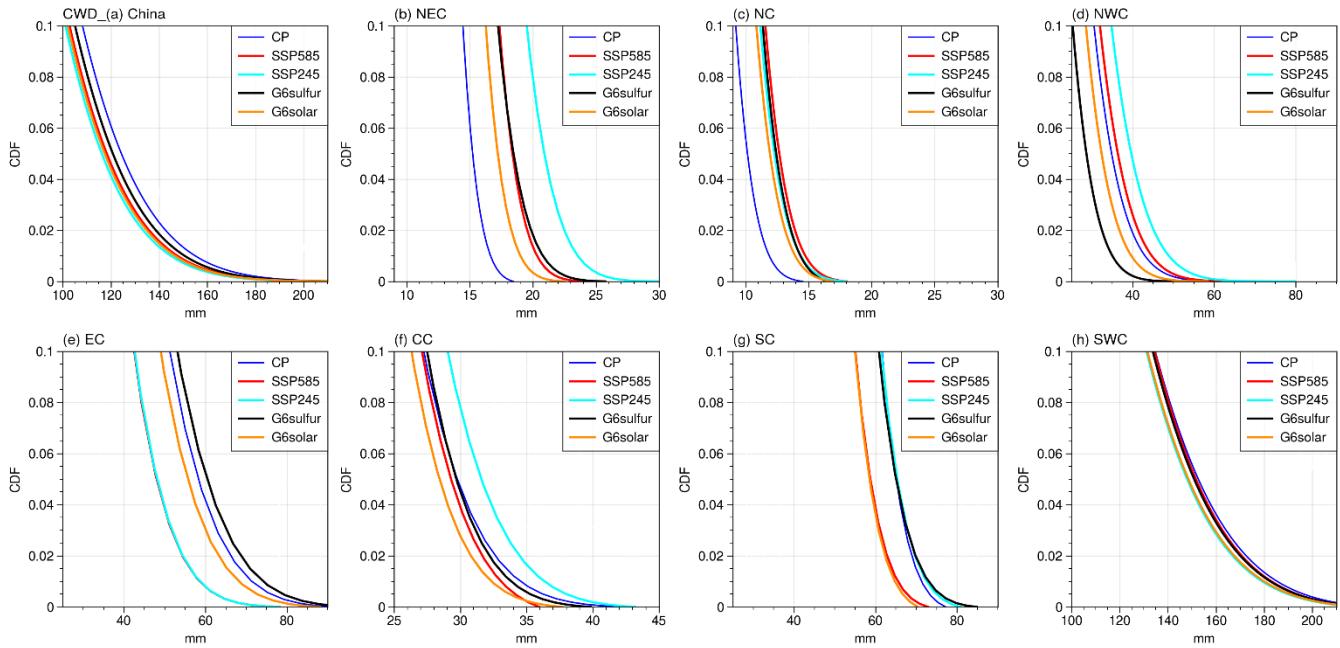


Figure 9. Same as Figure 6, but for CWD in China and 7 subregions.

460

In summary, CWD under SSP5-8.5 and SSP2-4.5 scenarios does not consistently exhibit simultaneously increases or decreases across all regions. CWD will significantly increase in QTP, and decrease in north China (almost in mid-latitudes, north of 30°N) but not serious in the future. The maximum increase occurs in SWC, SAI effectively ameliorates the decrease of CWD under SSP5-8.5 in southeast QTP (from about 90°E - 100°E). G6sulfur yields statistically similar outcome to that of SSP2-4.5 in NC and SC. SRM strategies yields results in R50mm nearly identical to those of the SSP2-4.5 scenario, and would have the most significant impact on weakening rainstorms in these densely populated regions. As the global mean temperature targets of G6sulfur, G6solar and SSP2-4.5 are nominally identical, this suggests that it is the global mean temperature change that is the dominant factor in driving changes in extreme precipitation.

465

3.2.2 Dry extreme changes

470 As for extreme wet indices, extreme dry conditions also occur in China, especially in north-western regions (Wang et al., 2017). The focus is on DD and CDD to study these changes and explore the impact of SAI.

For DD, the ensemble mean of UKESM simulations projects a significant increase (~~p-value < 0.05~~) in most of southern China (east of SWC, SC, and south of CC, EC) and a small part of western Xinjiang province (Fig.10a) for the SSP5-8.5 scenario (2071-2100) relative to the ~~PD~~control period (1981-2010). The largest increase, reaching up to 40 days, is observed in Fuzhou and Taiwan (southeast SC, near 120° E, 25°N). Decreases in DD are observed in northern and west China, including NEC, NC, NWC, west of SWC and north of CC, EC. Similar changes with smaller magnitudes are also observed under the SSP2-4.5 scenario (Fig.10b) and G6solar (Fig.10d). It is worth noting that, in comparison to the other three experiments, G6sulfur results in the most substantial increase in DD in western NWC (Fig.7c, Kunlun Mountains) in the future, indicating that G6sulfur exacerbates drought conditions in Kunlun Mountains. This may be related to topography and slope, both of which play important roles in glacier change in the Kunlun Mountains (Niu et al., 2023).

Under SSP5-8.5 warming conditions (Fig.10e), there is a significant CDD decrease (~~p-value < 0.05~~) in north-western and northern China, with the most significant decrease in NWC, consistent with Xu et al., (2019). This implies that ignoring rising temperatures seems to mitigate dry conditions (Xu et al., 2022a). In line with prior studies, there are notable north-south CDD variation in China (Feng et al., 2011).

485 The figure shows increased CDD in southern regions (along the middle and lower Yangtze River, south and parts of southwest China) but not significantly, hinting at potential increased droughts in southern China (Feng et al., 2011). These results also align with the predicted decrease in the north and increase in the south in CDD by RegCM4 (Ji and Kang, 2015) and PRECIS (Meng et al., 2021) models. Smaller CDD changes are observed in most regions under SSP2-4.5 (Fig.10f), G6sulfur (Fig.10g) and G6solar (Fig.10h). It worth noting that G6sulfur shows a slight future increase in western China (Tarim Basin).

490

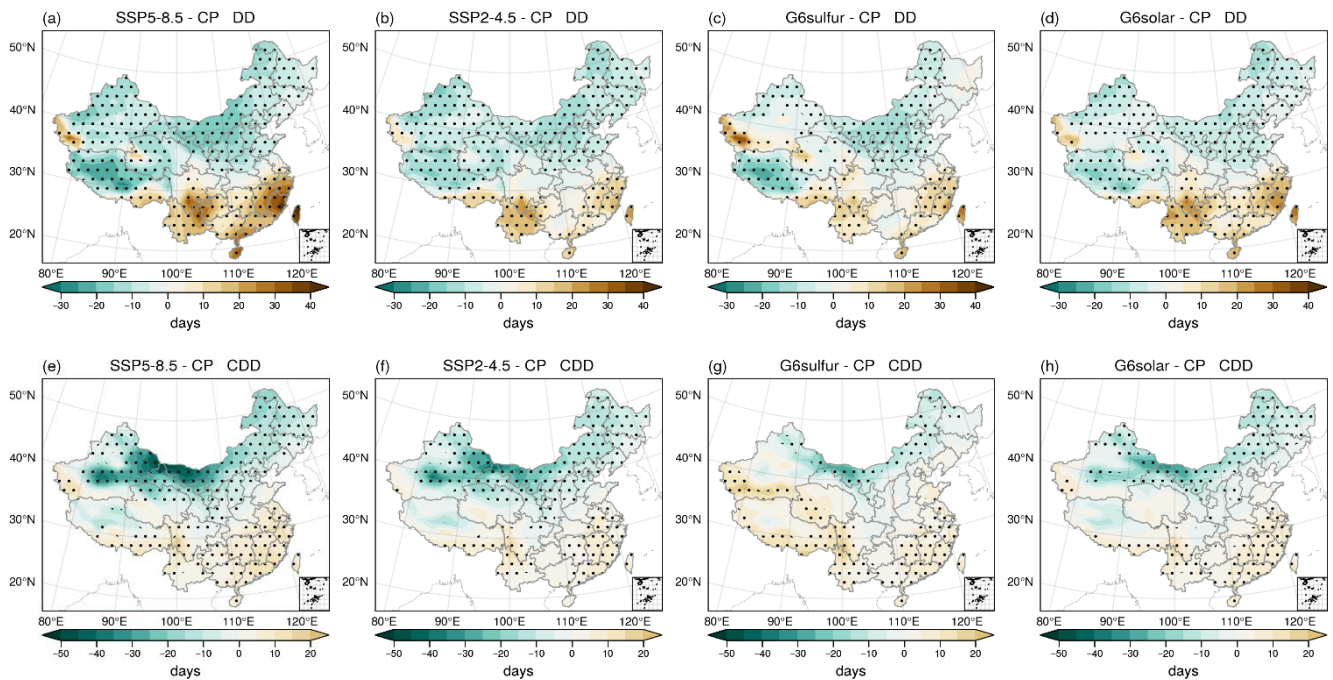


Figure 10. Same as Figure 4, but for (a-d) DD (days) and (e-h) CDD (days).

495 Fig.11 shows the impact of SAI on DD and CDD distribution in comparison to G6sulfur and other experiments. G6sulfur increases DD in northern and northwest China compared to SSP5-8.5 (Fig.11a), albeit mitigating the DD in a warmer climate (Fig.10c). Compared to SSP2-4.5 (Fig.11b), G6sulfur leads to a further increase in western China near 35°N, up to 25 days. However, G6sulfur reduces dry climate in the south China compared to other experiments, despite an increased drought risk (as seen in Fig.10a-d). Comparisons confirm that G6sulfur increases CDD in most inland areas of China compared to SSP5-
500 8.5 (Fig.11d), Only a few coastal areas show a reduction. G6sulfur increases the CDD almost across the entire China when compared to SSP2-4.5 (Fig.11e) and G6solar (Fig.11f).

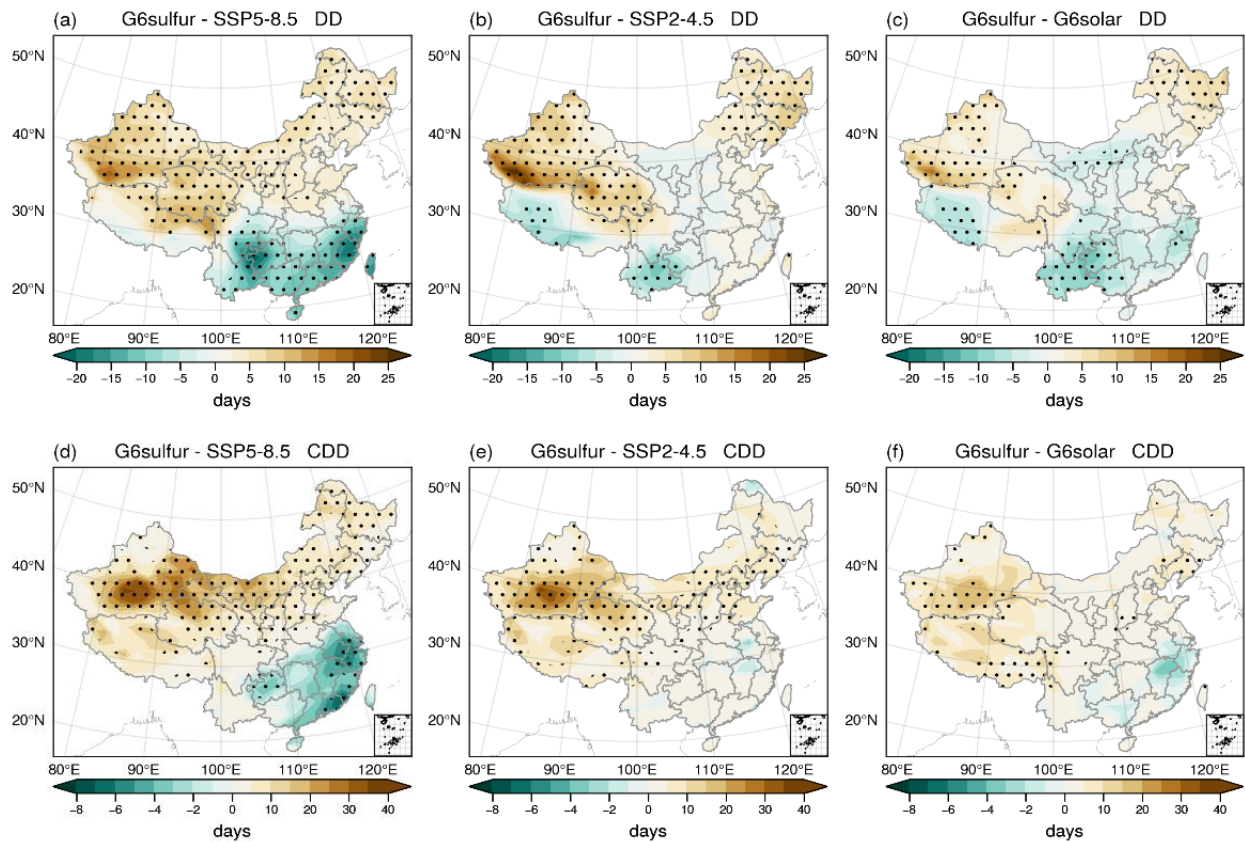


Figure 11. Same as Figure 5, but for (a-c) DD (days) and (d-f) CDD (days).

505

510

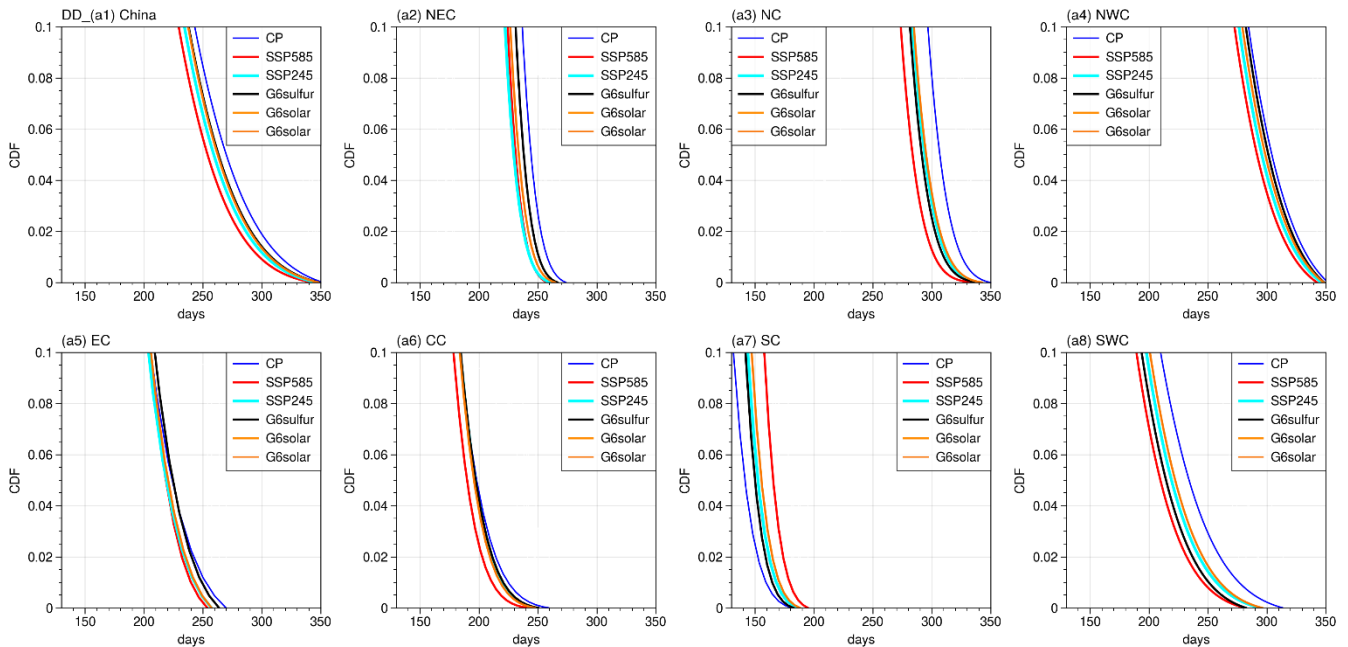
The tail of the DD CDFs in PDcontrol period (blue) is consistently shifts to the right compared to the other lines in NEC, NC, and NWC (Fig.12(a2) - (a4)), which corresponds to the declining trend (green shaded areas) in northern China as shown in Fig.10a-d. As shown in Table 3, the DD is positive in the SC region, meaning G6sulfur effectively lowers the threshold for extreme DD events compared to SSP5-8.5. This suggests that the SAI is more effective for DD maximum in the humid region. The black line surpasses the other three experiments in NWC, which explains the maximum increase value along Kunlun Mountains in NWC in Fig.10a-d and Fig.11a-c. It is noteworthy that in CC and SC, G6sulfur yields similar statistic results as SSP2-4.5.

515

The blue line surpasses the other four lines in NEC, NC and NWC, clarifying the decrease of CDD in the northern regions as evident in Fig.10e-h, signifying a reduced drought risk in northern China in the future. Conversely, the red line consistently stays to the left, while the black line is positioned to the right compared to the other G6 experiment lines. This suggests that G6sulfur and G6solar increase the drought risk when compared to the SSP5-8.5 scenario in northern regions, and the effect of

520 G6sulfur is more pronounced than that of G6solar. However, the distance between black and other G6 experiments lines is wider in NWC than in other regions, indicating the maximum increase in CDD under G6sulfur in NWC. This corresponds to the maximum differences in NWC in Fig.11d-f. It is worth noting that G6solar outperforms G6sulfur compared to SSP2-4.5 in China (except for SWC region) as the distance between the orange line and the cyan line is smaller than that between the black line and the cyan line. The positive value in Table 3 of the CDD index in the SC and SWC regions in Table 3 indicates that G6sulfur notably closes the threshold of CP extreme CDD events compared to SSP5-8.5, thereby approaching drought extremes of CP in these regions. This suggests that G6sulfur has the potential to mitigate the CDD extremes. The ameliorating effect of DD and CDD compared to SSP5-8.5 in the SC region under G6sulfur may be related to the strengthening of the anti-cyclonic circulation associated with the subtropical gyre, which appears to increase under G6 compared to SSP5-8.5 (Liang and Haywood, 2023). This intensification results in an increased inflow of moist air from the ocean at 850hPa and a greater supply of moisture to the southern region of the area.

525



530

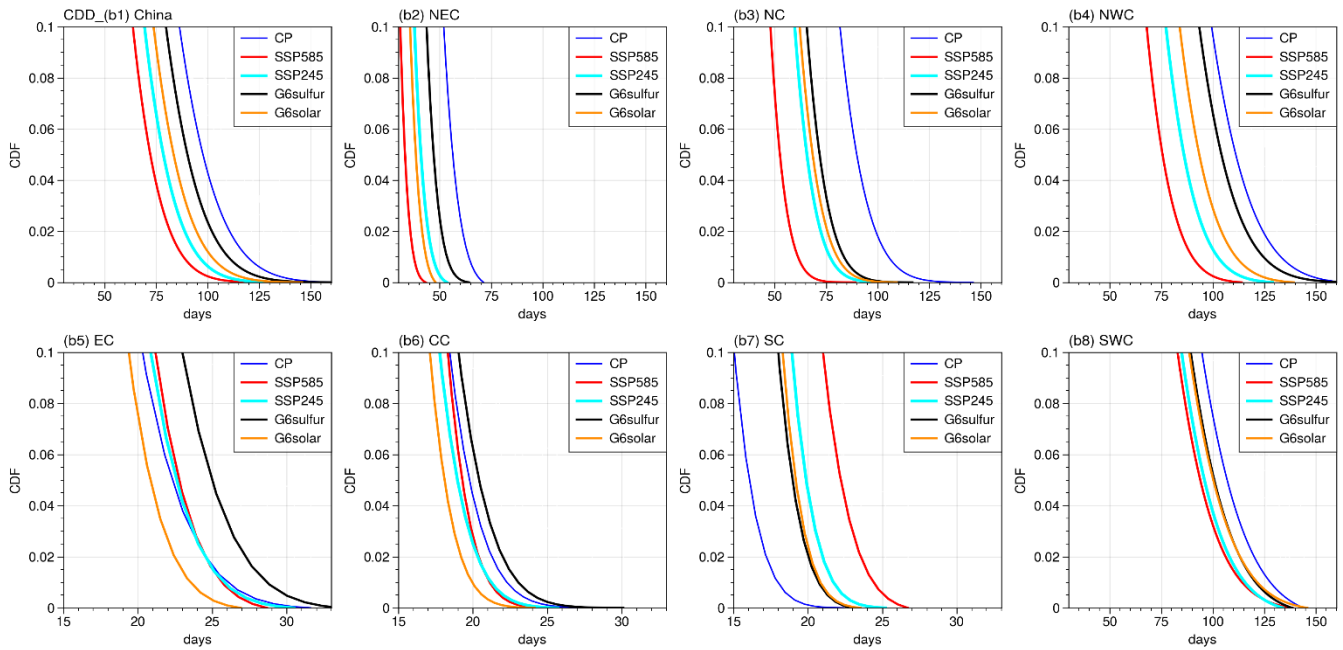


Figure 12. Same as Figure 6, but for DD (a1-a8) and CDD (b1-b8) in China and 7 subregions.

535 In summary, both DD and CDD projected increase in the south and southeast China but decrease in the north and northwest
 540 regions by the end of the 21st century in the four scenarios4-experiments. This reflects a potential decrease in drought risk in
 northwest regions and an increase in extreme drought events in low-latitude southeast coastal areas in the future according to
 four G6 simulations. Changes in precipitation will affect soil moisture, thereby influencing evapotranspiration (ET) and
 ultimately precipitation patterns. Assessing whether changes in DD and CDD affect drought risk also requires consideration
 of variations in ET and soil moisture (Cheng et al., 2019; Dagon and Schrag, 2016). Furthermore, solar radiation management
 (SRM) may increase drought risk in northern regions (NEC, NC, and NWC). This reflects declining drought risk in northwest
 545 regions and increased extreme drought events in low latitude southeast coastal areas in the future by G6 simulations. G6sulfur
 exacerbates drought conditions in Kunlun Mountains compared to other three experiments, and yields similar statistic results
 of DD as SSP2 4.5 in southeastern regions. SRM increase the drought risk when compared to SSP5 8.5 and SSP2 4.5 scenarios
 in northern regions (NEC, NC and NWC), and the effect of G6sulfur is more pronounced than that of G6solar. G6solar
 outperforms G6sulfur compared to SSP2 4.5 in China (except for SWC region).

4. Summary and discussion

In this study, based on simulations of the UKESM1, the effects of SAI on precipitation and the related extreme metrics are
 assessed over different sub-regions in China by comparing the results among different scenarios. We found that, under future

emission scenarios (SSP5-8.5 and SSP2-4.5), most of the sub-regions in China are projected to experience increased precipitation and extreme wet climate events by the end of 21st century, compared to the control period (1981-2010), particularly in the eastern and south-eastern coastal areas. Both the G6sulfur and G6solar show remarkable ameliorated changes in extreme rainfall intensity and frequency, and may abate most of the detrimental extremes that are evident under the SSP5-8.5 scenario. In general, the effects of the SRM experiments are similar to that of the SSP2-4.5. This suggests that the effects of SAI are encouraging, and can be seen as an effective option for mitigating flooding events, especially in the populated southeast areas. However, extreme drought events show an increase in some regions such as the north and northwest China compared with SSP5-8.5, implying the SRM may not be suitable for addressing drought risk in these regions. All the findings in our paper extend the current understating of extreme hydrological responses to climate change and SAI in China. The regional analysis presents new insights into identifying the vulnerable areas under hydrological changes and how they may benefit from the SRM.

the G6sulfur experiment with the high (SSP5 8.5) and medium (SSP2 4.5) levels of GHG emissions and solar constant reduction (G6solar) based on the coupled simulations of UKESM1. As both G6sulfur and G6solar aim to reduce future warming from the high-end GHG emission scenario (SSP5 8.5) to the medium GHG emission scenario (SSP2 4.5), the results reveal distinct responses of precipitation extreme indices to different statuses of external climate forcing. The conclusions of the paper are summarized as follows:

1. Under future warming scenarios (SSP5 8.5 and SSP2 4.5), most of sub-regions in China are projected to experience increased precipitation and extreme wet climate events by the end of 21st century, particularly in the eastern and south-eastern coastal areas. This aligns with the prior study that found significant increases in precipitation extremes under the SSP5 8.5 and SSP2 4.5 scenarios (Xu et al., 2022b). Research indicates that the future reduction in anthropogenic aerosol emissions is expected to significantly enhance East Asian summer monsoon circulation and precipitation, potentially contributing to the increased precipitation extremes across China (Wang et al., 2016). SSP5 8.5 high-emission scenario projects a strengthening of future precipitation, while the G6sulfur and G6solar show ameliorated changes in precipitation.

2. With respect to SSP5 8.5, SRM effectively mitigates the increases in extreme rainfall intensities (RX1day, RX5day, and R95p) and frequency (R50mm), especially in the populated southeast areas. For RX1day, G6sulfur provides statistical outcomes more similar than G6solar compared to SSP2 4.5 in NC. While G6solar provides statistical outcomes more similar than G6sulfur to those obtained from SSP2 4.5 in SWC. For R95p, G6solar provides statistically outcome more similar than G6sulfur to those obtained from SSP2 4.5 in EC, NC and SWC. SRM strategies weaken rainstorms in densely populated regions. SAI effectively ameliorates the decrease in CWD under SSP5 8.5 in southeast QTP (from about 90°E–100°E), and yields statistically similar outcome to those of SSP2 4.5 in NEC, NC, EC, and SC.

3. Simulations of extreme drought events show a projected increase in south and southeast China. While there has been an improvement in mitigating drought conditions in Kunlun Mountains and Tarim Basin, G6sulfur exacerbates drought conditions compared to the other three experiments. G6sulfur yields similar statistic results of DD as SSP2 4.5 in south-eastern regions

(EC, CC and SC). The increased drought risk under G6sulfur is more pronounced than that under G6solar in northern regions (NEC, NC and NWC) when compared to the SSP5-8.5 and SSP2-4.5 scenarios. G6solar outperforms G6sulfur compared to SSP2-4.5 in China (except for SC region). Additionally, in NC and SWC, G6solar provides statistically similar results to SSP2-4.5.

585 ~~The difference is shown in the magnitude as the use of SAI has more effects in reducing precipitation compared to solar constant reduction. The spatial patterns on extremely high and low precipitations under both intervention strategies are highly similar, in which this result aligns with the conclusions from (Visioni et al., 2022) on global extremes under SAI and solar constant reduction.~~

590 ~~It is projected that the intensification of the hydrological cycle evident under SSP5-8.5 will become less intensified under both types of SRM in China. Previous studies, including (Niemeier et al., 2013) and (Ji et al., 2018), highlighted that the precipitation reduction response is robust under the SRM strategies. Our results of ETDCCI indices related to extreme precipitation and heavy rainfalls have concluded that SAI is mainly effective in mitigation in southeastern and southern China. The regions under the influence cover many important economic centres and port cities in China that are coastal and experience a high level of flooding risk. The use of SAI can be seen as a future option for preventing major flooding events. While both SRM strategies effectively reduce drying changes in most northern and western China, their implementation leads to an increased risk of drought within these regions compared to the SSP5-8.5 and SSP2-4.5 scenarios. Overall, our study shows efficacy of SAI in mitigating wet extremes in China. However, it highlights the unsuitability of SRM strategies for addressing drought risk in the northern and western regions.~~

600 As this study is solely focused on the precipitation and relevant extreme events based on the models, we cannot take socio-economic, biological, and other factors into account. Although many studies have also focused on areas such as crops (Cheng et al., 2019) and important modes of natural variability (Jones et al., 2020), they are mostly targeted on a wider and global scale, more regional analysis on China still requires future research. Also, the climate models and data remain uncertain, indicating the continuous improvements are needed in models for simulations in deterring the future pathways of climate change and SRM. ~~(Visioni et al., 2021)All the findings and conclusions in our paper extend the current understating of extreme hydrological responses to climate change and SAI in China. The regional analysis presents new insights into identifying the vulnerable areas under hydrological changes and how they may benefit from the SRM. (Bednarz et al., 2022). We~~ In addition, it should be noted that, owing to the second-order nature of the changes in climate extremes when compared to SSP2-4.5 (i.e. a relatively small signal to noise when compared to those from SSP5-8.5), that the analysis is very dependent on the model used in the analysis (UKESM1); other models may produce significantly different results. Additionally, reducing the solar constant within climate models also triggers a dynamic reaction in the stratosphere (Bednarz et al., 2022). It is therefore crucial to perform similar analyses with other state-of-the-art climate models to elucidate the robustness of the results, and to inform

615 policymakers of any potential detrimental influences of SRM. ~~The general message appears to be that both the G6sulfur and G6solar simulations abate most of the changes in detrimental extremes that are evident under the SSP5-8.5 scenario. Changes in extreme precipitation under G6sulfur and G6solar for all precipitation variables bar the consecutive wet days (CWD; where negligible changes occur compared to present day conditions occur in NEC and EC regions and a increase in NWC) show only subtle second order differences as compared to SSP2-4.5. As the global mean temperature targets of G6sulfur, G6solar and SSP2-4.5 are nominally identical, this suggests that it is the global mean temperature change that is the dominant factor in driving changes in extreme precipitation.~~

620 While the general amelioration of precipitation changes under SAI might seem a somewhat obvious conclusion owing to the spin-down of the hydrological cycle under cooler temperatures (e.g. Tilmes et al, 2013), other studies have shown large-scale climatic shifts in key modes of climate variability that impact precipitations. For example, Haywood et al. (2013) and Jones et al. (2017) have modelled significant detrimental impacts on Sahelian precipitation and north Atlantic hurricane frequency under non-judicious SAI implementation owing to large-scale shifts in the Inter-Tropical Convergence Zone. Multi-model SAI simulations Jones et al. (2020, 2021) have shown detrimental impacts on the North Atlantic Oscillation leading to rainfall 625 deficits over the Iberian Peninsula above and beyond those evident in SSP5-8.5. Similarly, recent simulations of non-judicious deployment of an alternate SRM technique, that of marine cloud brightening, locked the climate into an extremely strong permanent La-Nina-like phase with associated detrimental impacts on sea-level rise over low-lying South Pacific islands (Haywood et al., 2023). It appears that, over large areas of China, any changes in detrimental extremes in precipitation are second order when compared to the benefits associated with reducing global mean temperatures. ~~For dry days that influence 630 drought (i.e. the DD and CDD diagnostics), the situation is rather different with increased dry days and continuous dry days as compared to SSP5-8.5. Again, this is consistent with SRM activities spinning down the hydrological cycle (e.g. Tilmes et al., 2013)~~

635 To conclude, it appears that changes in precipitation extremes related to flooding over the bulk of China that are induced under climate change may be abated by SRM, but changes in dry days relating to drought are likely to be enhanced. Large-scale shifts in precipitation patterns associated with changes in atmospheric dynamics noted in other SRM studies using climate models developed by the Hadley Centre (e.g. HadGEM2, UKESM1; Haywood et al., 2013, 2023; Jones et al., 2017; Jones et al., 2020; 2021) do not appear to impact the bulk of China. Based on the same set of simulations as this paper, the study by Liang and Haywood (2023) demonstrated apparent side-effects of SRM as the simulated SAI scenario exacerbates the weakening the subtropical westerly jet and further enhance the mid-latitude precipitation over China by modulating 640 atmospheric rivers over East Asia. Of course, we stress that the results from these simulations are model specific and further work with other models needs to be performed to understand the robustness of these conclusions more generally.

Code and data availability

All the UKESM1 model data for the SSP5-8.5, SSP2-4.5, GeoMIP G6sulfur and GeoMIP G6solar scenarios used in this work are available from the Earth System Grid Federation (WCRP, 2022; <https://esgf-node.llnl.gov/projects/cmip6>). The APHRODITE data have been downloaded from their official website, which is managed by the Data Integration and Analysis System (DIAS, 2022; https://search.diasjp.net/en/dataset/APHRO_MA).

Supplement

The supplement related to this article is available online at:

Author contributions

The majority of this work was completed when OW was visiting the University of Exeter in the UK under a scholarship from the China Scholarship Council. JL and JH devised the experiment, led the analysis. OW wrote the paper with contributions from all the co-authors.

Competing interests

The contact authors have declared that neither of the authors has any competing interests.

Disclaimer

Publisher's note: Copernicus Publications remains neutral with regard to jurisdictional claims in published maps and institutional affiliations.

Acknowledgements

We are grateful to the University of Exeter for providing the academic platform for this study and the Met Office for doing the numerical calculations in this work. The authors thank Andy Jones, for help with running the G6sulfur and G6solar experiments.

Reference

Apurv, T., Mehrotra, R., Sharma, A., Goyal, M. K., and Dutta, S.: Impact of climate change on floods in the Brahmaputra basin using CMIP5 decadal predictions, *J. Hydrol.*, 527, 281-291, <https://doi.org/10.1016/j.jHydrol.2015.04.056>, 2015.

665 Archibald, A. T., O'Connor, F. M., Abraham, N. L., Archer-Nicholls, S., Chipperfield, M. P., Dalvi, M., Folberth, G. A., Dennison, F., Dhomse, S. S., and Griffiths, P. T.: Description and evaluation of the UKCA stratosphere–troposphere chemistry scheme (StratTrop vn 1.0) implemented in UKESM1, *Geosci. Model Dev.*, 13, 1223-1266, <https://doi.org/10.5194/gmd-13-1223-2020>, 2020.

670 [Bednarz, E. M., Visioni, D., Banerjee, A., Braesicke, P., Kravitz, B., and MacMartin, D. G.: The Overlooked Role of the Stratosphere Under a Solar Constant Reduction, *Geophys. Res. Lett.*, 49, e2022GL098773, <https://doi.org/10.1029/2022GL098773>, 2022.](https://doi.org/10.1029/2022GL098773)

Bluth, G. J., Doiron, S. D., Schnetzler, C. C., Krueger, A. J., and Walter, L. S.: Global tracking of the SO₂ clouds from the June, 1991 Mount Pinatubo eruptions, *Geophys Res Lett.*, 19, 151-154, <https://doi.org/10.1029/91GL02792>, 1992.

~~Cao, L.: The effects of solar radiation management on the carbon cycle, *Curr. Clim. Change Rep.*, 4, 41-50, <https://doi.org/10.1007/s40641-018-0088-z>, 2018.~~

680 CDF vs PDF: What's the Difference?: <https://www.analyticsvidhya.com/blog/2023/07/cdf-vs-pdf/>, last access: 15 November 2023.

CDP. 2023 China Floods.: The summer of 2023 has seen unprecedented flooding across China as monsoon season, typhoons and intense rainfall have battered the country. <https://disasterphilanthropy.org/disasters/2023-china-floods/>, last access: 10 November 2023.

685 Cheng, W., MacMartin, D. G., Dagon, K., Kravitz, B., Tilmes, S., Richter, J. H., Mills, M. J., and Simpson, I. R.: Soil moisture and other hydrological changes in a stratospheric aerosol geoengineering large ensemble, *J. Geophys. Res.-Atmos.*, 124, 12773-12793, <https://doi.org/10.1029/2018JD030237>, 2019.

690 Deng, L., Feng, J., Zhao, Y., Bao, X., Huang, W., Hu, H., and Duan, Y.: The remote effect of binary Typhoon Infa and Cempaka on the “21.7” heavy rainfall in Henan Province, China, *J. Geophys. Res.-Atmos.*, 127, e2021JD036260, <https://doi.org/10.1029/2021JD036260>, 2022.

Dong, B., Xia, J., Li, Q., and Zhou, M.: Risk assessment for people and vehicles in an extreme urban flood: Case study of the “7.20” flood event in Zhengzhou, China, *Int. J. Disaster Risk Reduct.*, 80, 103205, <https://doi.org/10.1016/j.ijdr.2022.103205>, 2022.

Eyring, V., Bony, S., Meehl, G. A., Senior, C. A., Stevens, B., Stouffer, R. J., and Taylor, K. E.: Overview of the Coupled Model Intercomparison Project Phase 6 (CMIP6) experimental design and organization, *Geosci. Model Dev.*, 9, 1937-1958, 700 <https://doi.org/10.5194/gmd-9-1937-2016>, 2016.

Feng, L., Zhou, T., Wu, B., Li, T., and Luo, J.-J.: Projection of future precipitation change over China with a high-resolution global atmospheric model, *Adv. Atmos. Sci.*, 28, 464-476, <https://doi.org/10.1007/s00376-010-0016-1>, 2011.

705 Frich, P., Alexander, L. V., Della-Marta, P., Gleason, B., Haylock, M., Tank, A. K., and Peterson, T.: Observed coherent changes in climatic extremes during the second half of the twentieth century, *Clim. Res.*, 19, 193-212, <https://doi.org/10.3354/cr019193>, 2002.

Haywood, J. M., Jones, A., and Jones, G. S.: The impact of volcanic eruptions in the period 2000–2013 on global mean 710 temperature trends evaluated in the HadGEM2-ES climate model, *Atmos. Sci. Lett.*, 15, 92-96, <https://doi.org/10.1002/asl2.471>, 2014.

Haywood, J. M., Jones, A., Johnson, B. T., and McFarlane Smith, W.: Assessing the consequences of including aerosol absorption in potential stratospheric aerosol injection climate intervention strategies, *Atmos. Chem. Phys.*, 22, 6135-6150, 715 <https://doi.org/10.5194/acp-22-6135-2022>, 2022.

Held, I. M. and Soden, B. J.: Robust responses of the hydrological cycle to global warming, *J. Climate.*, 19, 5686-5699, <https://doi.org/10.1175/JCLI3990.1>, 2006.

720 Huang, R., Chen, J., and Huang, G.: Characteristics and variations of the East Asian monsoon system and its impacts on climate disasters in China, *Adv. Atmos. Sci.*, 24, 993-1023, <https://doi.org/10.1007/s00376-007-0993-x>, 2007.

Imai, Y., Meyer, K. J., Iinishi, A., Favre-Godal, Q., Green, R., Manuse, S., Caboni, M., Mori, M., Niles, S., and Ghiglieri, M.: A pause in Southern Hemisphere circulation trends due to the Montreal Protocol, *Nature*, 579(7800), 544-548, 725 <https://doi.org/10.1038/s41586-020-2120-4>, 2020.

IPCC, C. C. The Physical Science Basis. Contribution of Working Group I to the 6th Assessment Report, 2021.

IPCC – Intergovernmental Panel on Climate Change: Global warming of 1.5 °C, in: An IPCC Special Report on the impacts 730 of global warming of 1.5 °C above pre-industrial levels and related global greenhouse gas emission pathways, in the context of strengthening the global response to the threat of climate change, sustainable development, and efforts to eradicate poverty,

edited by: Masson-Delmotte, V., Zhai, P., Pörtner, H. O., Roberts, D., Skea, J., Shukla, P. R., Pirani, A., Moufouma-Okia, W., Péan, C., Pidcock, R., Connors, S., Matthews, J. B. R., Chen, Y., Zhou, X., Gomis, M. I., Lonnoy, E., Maycock, T., Tignor, M., and Waterfield, T., <https://www.ipcc.ch/sr15/> (last access: 22 September 2022), 2018.

735

[Irvine, P. J., Kravitz, B., Lawrence, M. G., and Muri, H.: An overview of the Earth system science of solar geoengineering, *WIREs Climate Change*, 7, 815–833, <https://doi.org/10.1002/wcc.423>, 2016.](#)

740 Ji, D., Fang, S., Curry, C. L., Kashimura, H., Watanabe, S., Cole, J. N., Lenton, A., Muri, H., Kravitz, B., and Moore, J. C.: Extreme temperature and precipitation response to solar dimming and stratospheric aerosol geoengineering, *Atmos. Chem. Phys.*, 18, 10133–10156, <https://doi.org/10.5194/acp-18-10133-2018>, 2018.

Ji, Z. and Kang, S.: Evaluation of extreme climate events using a regional climate model for China, *Int. J. Climatol.*, 35, 888–902, <https://doi.org/10.1002/joc.4024>, 2015.

745

Jia, H., Chen, F., Pan, D., Du, E., Wang, L., Wang, N., and Yang, A.: Flood risk management in the Yangtze River basin—Comparison of 1998 and 2020 events, *Int. J. Disaster Risk Reduct.*, 68, 102724, <https://doi.org/10.1016/j.ijdrr.2021.102724>, 2022.

750 Jones, A. C., Hawcroft, M. K., Haywood, J. M., Jones, A., Guo, X., and Moore, J. C.: Regional climate impacts of stabilizing global warming at 1.5 K using solar geoengineering, *Earth's Future*, 6, 230–251, <https://doi.org/10.1002/2017EF000720>, 2018.

755 Jones, A., Haywood, J. M., Jones, A. C., Tilmes, S., Kravitz, B., and Robock, A.: North Atlantic Oscillation response in GeoMIP experiments G6solar and G6sulfur: why detailed modelling is needed for understanding regional implications of solar radiation management, *Atmos. Chem. Phys.*, 21, 1287–1304, <https://doi.org/10.5194/acp-21-1287-2021>, 2021.

Kravitz, B., Robock, A., Boucher, O., Schmidt, H., Taylor, K. E., Stenchikov, G., and Schulz, M.: The geoengineering model intercomparison project (GeoMIP), *Atmos. Sci. Lett.*, 12, 162–167, 2011.

760 Kravitz, B., Caldeira, K., Boucher, O., Robock, A., Rasch, P. J., Alterskjaer, K., Karam, D. B., Cole, J. N., Curry, C. L., and Haywood, J. M.: Climate model response from the geoengineering model intercomparison project (GeoMIP), *J. Geophys. Res.-Atmos.*, 118, 8320–8332, <https://doi.org/10.1002/jgrd.50646>, 2013.

- 765 Kravitz, B., Robock, A., Tilmes, S., Boucher, O., English, J. M., Irvine, P. J., Jones, A., Lawrence, M. G., MacCracken, M.,
and Muri, H.: The geoengineering model intercomparison project phase 6 (GeoMIP6): Simulation design and preliminary
results, *Geosci. Model Dev.*, 8, 3379-3392, <https://doi.org/10.5194/gmd-8-3379-2015>, 2015.
- 770 [Klein Tank, A. M. G., Zwiers, F. W., and Zhang, X.: Guidelines on Analysis of extremes in a changing climate in support of
informed decisions for adaptation, in: Climate Data and Monitoring, \(WCDMP-No. 72; p. 52\), World Meteorological
Organization, \[https://library.wmo.int/doc_num.php?explnum_id=9419\]\(https://library.wmo.int/doc_num.php?explnum_id=9419\) \(last access: 24 August 2022\), 2009.](https://library.wmo.int/doc_num.php?explnum_id=9419)
- Lai, S., Xie, Z., Bueh, C., and Gong, Y.: Fidelity of the APHRODITE dataset in representing extreme precipitation over Central
Asia, *Adv. Atmos. Sci.*, 37, 1405-1416, <https://doi.org/10.1007/s00376-020-0098-3>, 2020.
- 775 Lee, H., Muri, H., Ekici, A., Tjiputra, J., and Schwinger, J.: The response of terrestrial ecosystem carbon cycling under different
aerosol-based radiation management geoengineering, *Earth Syst. Dynam.*, 12, 313-326, <https://doi.org/10.5194/esd-12-313-2021>, 2021.
- Li, S., Jiang, D., Lian, Y., and Yao, Y.: Interdecadal variations of cold air activities in Northeast China during springtime, *J.*
780 *Meteorol. Res.*, 30, 645-661, <https://doi.org/10.1007/s13351-016-5912-6>, 2016.
- Liang, J. and Haywood, J.: Future changes in atmospheric rivers over East Asia under stratospheric aerosol intervention, *Atmos.*
Chem. Phys., 23, 1687-1703, <https://doi.org/10.5194/acp-23-1687-2023>, 2023.
- 785 Liang, J., Meng, C., Wang, J., Pan, X., and Pan, Z.: Projections of mean and extreme precipitation over China and their
resolution dependence in the HighResMIP experiments, *Atmos. Res.*, 293, 106932,
<https://doi.org/10.1016/j.atmosres.2023.106932>, 2023.
- Liu, Z., Lang, X., and Jiang, D.: Impact of stratospheric aerosol injection geoengineering on the summer climate over East
790 Asia, *J. Geophys. Res.-Atmos.*, 126, e2021JD035049, <https://doi.org/10.1029/2021JD035049>, 2021.
- Liu, Z., Lang, X., Miao, J., and Jiang, D.: Impact of Stratospheric Aerosol Injection on the East Asian Winter Monsoon,
Geophys. Res. Lett., 50, e2022GL102109, <https://doi.org/10.1029/2022GL102109>, 2023.
- 795 McLandress, C., Shepherd, T. G., Scinocca, J. F., Plummer, D. A., Sigmond, M., Jonsson, A. I., and Reader, M. C.: Separating
the dynamical effects of climate change and ozone depletion. Part II: Southern Hemisphere troposphere, *J. Climate.*, 24, 1850-
1868, <https://doi.org/10.1175/2010JCLI3958.1>, 2011.

Meinshausen, M., Nicholls, Z. R., Lewis, J., Gidden, M. J., Vogel, E., Freund, M., Beyerle, U., Gessner, C., Nauels, A., and
800 Bauer, N.: The shared socio-economic pathway (SSP) greenhouse gas concentrations and their extensions to 2500, *Geosci.
Model Dev.*, 13, 3571-3605, <https://doi.org/10.5194/gmd-13-3571-2020>, 2020.

Meng, C., Zhang, L., Gou, P., Huang, Q., Ma, Y., Miao, S., Ma, W., and Xu, Y.: Assessments of future climate extremes in
China by using high-resolution PRECIS 2.0 simulations, *Theor. Appl. Climatol.*, 145, 295-311,
805 <https://doi.org/10.1007/s00704-021-03618-9>, 2021.

Mulcahy, J. P., Jones, C., Sellar, A., Johnson, B., Boutle, I. A., Jones, A., Andrews, T., Rumbold, S. T., Mollard, J., Bellouin,
N., Johnson, C. E., Williams, K. D., Grosvenor, D. P., and McCoy, D. T.: Improved Aerosol Processes and Effective Radiative
Forcing in HadGEM3 and UKESM1, *J. Adv. Model. Earth Sy.*, 10, 2786–2805, <https://doi.org/10.1029/2018MS001464>, 2018.

810

Niemeier, U., Schmidt, H., Alterskjær, K., and Kristjánsson, J.: Solar irradiance reduction via climate engineering: Impact of
different techniques on the energy balance and the hydrological cycle, *J. Geophys. Res.-Atmos.*, 118, 11,905-911,917,
<https://doi.org/10.1002/2013JD020445>, 2013.

815 Niu, S., Sun, M., Wang, G., Wang, W., Yao, X., and Zhang, C.: Glacier Change and Its Influencing Factors in the Northern
Part of the Kunlun Mountains, *Remote Sens.*, 15, 3986, <https://doi.org/10.3390/rs15163986>, 2023.

O’neill, B., Tebaldi, C., Van Vuuren, D., Eyring, V., Friedlingstein, P., Hurtt, G., Knutti, R., Kriegler, E., Lamarque, J., and
Lowe, J.: The Scenario Model Intercomparison Project (ScenarioMIP) for CMIP6, *Geosci. Model Dev.*, 9, 3461–3482,
820 <https://doi.org/10.5194/gmd-9-3461-2016>, 2016.

Peng, Y., Zhao, X., Wu, D., Tang, B., Xu, P., Du, X., and Wang, H.: Spatiotemporal variability in extreme precipitation in
China from observations and projections, *Water*, 10, 1089, <https://doi.org/10.3390/w10081089>, 2018.

825 Pinto, I., Jack, C., Lennard, C., Tilmes, S., and Odoulami, R. C.: Africa's climate response to solar radiation management with
stratospheric aerosol, *Geophys. Res. Lett.*, 47, e2019GL086047, <https://doi.org/10.1029/2019GL086047>, 2020.

Plazzotta, M., Séférian, R., and Douville, H.: Impact of Solar Radiation Modification on Allowable CO2 Emissions: What Can
We Learn From Multimodel Simulations?, *Earth’s Future*, 7, 664–676, <https://doi.org/10.1029/2019EF001165>, 2019.

830

Qi, Y., Yu, H., Fu, Q., Chen, Q., Ran, J., and Yang, Z.: Future changes in drought frequency due to changes in the mean and shape of the PDSI probability density function under RCP4. 5 scenario, *Front Earth Sci*, 10, 386, <https://doi.org/10.3389/feart.2022.857885>, 2022.

835 [Qin, P. and Xie, Z.: Detecting changes in future precipitation extremes over eight river basins in China using RegCM4 downscaling, *J. Geophys. Res.-Atmos.*, 121, 6802-6821, <https://doi.org/10.1002/2016JD024776>, 2016.](#)

Rana, A., Madan, S., and Bengtsson, L.: Performance evaluation of regional climate models (RCMs) in determining precipitation characteristics for Gothenburg, Sweden, *Hydrol. Res.*, 45, 703-714, <https://doi.org/10.2166/nh.2013.160>, 2013.

840

Rao, C., Chen, G., and Ran, L.: Effects of Typhoon In-Fa (2021) and the Western Pacific Subtropical High on an Extreme Heavy Rainfall Event in Central China, *J. Geophys. Res.-Atmos.*, 128, e2022JD037924, <https://doi.org/10.1029/2022JD037924>, 2023.

845 REUTERS: FACTBOX Impact of floods in China after Typhoon Doksuri, <https://www.reuters.com/world/asia-pacific/impact-floods-china-after-typhoon-doksuri-2023-08-11/>, last access: 11 November 2023.

Robock, A.: Volcanic eruptions and climate, *Rev. Geophys.*, 38, 191-219, <https://doi.org/10.1029/1998RG000054>, 2000. Schmidt, A., Mills, M. J., Ghan, S., Gregory, J. M., Allan, R. P., Andrews, T., Bardeen, C. G., Conley, A., Forster, P. M., and Gettelman, A.: Volcanic radiative forcing from 1979 to 2015, *J. Geophys. Res.-Atmos.*, 123, 12491-12508, <https://doi.org/10.1029/2018JD028776>, 2018.

Self, S., Zhao, J.-X., Holasek, R. E., Torres, R. C., and King, A. J.: The atmospheric impact of the 1991 Mount Pinatubo eruption, in: *Fire and Mud: Eruptions and lahars of Mount Pinatubo*, Philippines, University of Washington Press, 1996. Sellar, 855 A., Jones, C. G., Mulcahy, J. P., Tang, Y., Yool, A., Wiltshire, A., O'Connor, F. M., Stringer, M., Hill, R., Palmieri, J., Woodward, S., de Mora, L., Kuhlbrodt, T., Rumbold, S., Kelley, D. I., Ellis, R., Johnson, C. E., Walton, J., Abraham, N. L., Andrews, M. B., Andrews, T., Archibald, A. T., Berthou, S., Burke, E., Blockley, E., Carslaw, K., Dalvi, M., Edwards, J., Folberth, G. A., Gedney, N., Griffiths, P. T., Harper, A. B., Hendry, M. A., Hewitt, A. J., Johnson, B., Jones, A., Jones, C. D., Keeble, J., Liddicoat, S., Morgenstern, O., Parker, R. J., Predoi, V., Robertson, E., Siahann, A., Smith, R. S., Swaminathan, 860 R., Woodhouse, M., Zeng, G., and Zerroukat, M.: UKESM1: Description and evaluation of the UK Earth System Model, *J. Adv. Model. Earth Sy.*, 11, 4513–4558, <https://doi.org/10.1029/2019MS001739>, 2019.

865 [Simpson, I. S., S. Tilmes, Richter, J. H., Kravitz, B., MacMartin, D. G., Mills, M. J., Fasullo, J. T., and Pendergrass, A. G.: The regional hydroclimate response to stratospheric sulfate geoengineering and the role of stratospheric heating, *J. Geophys. Res.-Atmos.*, 124, 12587–12616, 2019.](#)

Soden, B. J., Wetherald, R. T., Stenchikov, G. L., and Robock, A.: Global cooling after the eruption of Mount Pinatubo: A test of climate feedback by water vapor, *Science*, 296, 727-730, <https://doi.org/10.1126/science.296.5568.727>, 2002.

870 Stenchikov, G. L., Kirchner, I., Robock, A., Graf, H. F., Antuna, J. C., Grainger, R. G., Lambert, A., and Thomason, L.: Radiative forcing from the 1991 Mount Pinatubo volcanic eruption, *J. Geophys. Res.-Atmos.*, 103, 13837-13857, <https://doi.org/10.1029/98JD00693>, 1998.

Storkey, D., Blaker, A. T., Mathiot, P., Megann, A., Aksenov, Y., Blockley, E. W., Calvert, D., Graham, T., Hewitt, H. T., and Hyder, P.: UK Global Ocean GO6 and GO7: A traceable hierarchy of model resolutions, *Geosci. Model Dev.*, 11, 3187-3213, 875 <https://doi.org/10.5194/gmd-11-3187-2018>, 2018.

Sui, Y., Lang, X., and Jiang, D.: Projected signals in climate extremes over China associated with a 2 C global warming under two RCP scenarios, *Int. J. Climatol.*, 38, e678-e697, <https://doi.org/10.1002/joc.5399>, 2018.

880 Sunilkumar, K., Yatagai, A., and Masuda, M.: Preliminary evaluation of GPM-IMERG rainfall estimates over three distinct climate zones with APHRODITE, *Earth. Sp. Sci.*, 6, 1321-1335, <https://doi.org/10.1029/2018EA000503>, 2019.

Tabari, H.: Climate change impact on flood and extreme precipitation increases with water availability. *Sci. Rep.*, 10: 13768, 885 <https://doi.org/10.1038/s41598-020-70816-2>, 2020.

Tang, B., Hu, W., and Duan, A.: Future projection of extreme precipitation indices over the Indochina Peninsula and South China in CMIP6 models, *J. Climate.*, 34, 8793-8811, <https://doi.org/10.1175/JCLI-D-20-0946.1>, 2021.

890 [Tew, Y. L., Tan, M. L., Liew, J., Chang, C. K., & Muhamad, N.: A review of the effects of solar radiation management on hydrological extremes, *Earth Environ.*, 1238, 1, <https://doi.org/10.1088/1755-1315/1238/1/012030>, 2023.](#)

~~Tank, A. K., Wijngaard, J., Können, G., Böhm, R., Demarée, G., Gocheva, A., Miletta, M., Pashiardis, S., Heijerlik, L., and Kern Hansen, C.: Daily surface air temperature and precipitation dataset 1901–1999 for European Climate Assessment (ECA), *Int. J. Climatol.*, 22, 1441–1453, 2002.~~

895

Tung, Y.-S., Wang, C.-Y., Weng, S.-P., and Yang, C.-D.: Extreme index trends of daily gridded rainfall dataset (1960–2017) in Taiwan, *Terr. Atmos. Oceanic Sci.*, 33, 8, <https://doi.org/10.1007/s44195-022-00009-z>, 2022.

900 [Tye, M. R., Dagon, K., Molina, M. J., Richter, J. H., Vioni, D., Kravitz, B., and Tilmes, S.: Indices of extremes: geographic patterns of change in extremes and associated vegetation impacts under climate intervention, *Earth Syst. Dynam.*, 13, 1233–1257, <https://doi.org/10.5194/esd-13-1233-2022>, 2022.](https://doi.org/10.5194/esd-13-1233-2022)

905 Vioni, D., Jones, A., Haywood, J., Séférian, R., Nabat, P., Boucher, O., Bednarz, E. M., and Niemeier, U.: Stratospheric ozone response to sulfate aerosol and solar dimming climate interventions based on the G6 Geoengineering Model Intercomparison Project (GeoMIP) simulations, *Atmos. Chem. Phys.*, 22, 4557–4579, <https://doi.org/10.5194/acp-22-4557-2022>, 2022.

910 Vioni, D., MacMartin, D. G., Kravitz, B., Boucher, O., Jones, A., Lurton, T., Martine, M., Mills, M. J., Nabat, P., and Niemeier, U.: Identifying the sources of uncertainty in climate model simulations of solar radiation modification with the G6sulfur and G6solar Geoengineering Model Intercomparison Project (GeoMIP) simulations, *Atmos. Chem. Phys.*, 21, 10039–10063, <https://doi.org/10.5194/acp-21-10039-2021>, 2021.

915 Walters, D., Baran, A. J., Boutle, I., Brooks, M., Earnshaw, P., Edwards, J., Furtado, K., Hill, P., Lock, A., Manners, J., Morcrette, C., Mulcahy, J., Sanchez, C., Smith, C., Stratton, R., Tennant, W., Tomassini, L., Van Weverberg, K., Vosper, S., Willett, M., Browse, J., Bushell, A., Carslaw, K., Dalvi, M., Essery, R., Gedney, N., Hardiman, S., Johnson, B., Johnson, C., Jones, A., Jones, C., Mann, G., Milton, S., Rumbold, H., Sellar, A., Ujiie, M., Whittall, M., Williams, K., and Zerroukat, M.: The Met Office Unified Model Global Atmosphere 7.0/7.1 and JULES Global Land 7.0 configurations, *Geosci. Model Dev.*, 12, 1909–1963, <https://doi.org/10.5194/gmd-12-1909-2019>, 2019

920 Wang, X., Pang, G., and Yang, M.: Precipitation over the Tibetan Plateau during recent decades: a review based on observations and simulations, *Int. J. Climatol.*, 38, 1116–1131, <https://doi.org/10.1002/joc.5246>, 2018.

925 Wang, Y., Zhou, B., Qin, D., Wu, J., Gao, R., and Song, L.: Changes in mean and extreme temperature and precipitation over the arid region of northwestern China: Observation and projection, *Adv. Atmos. Sci.*, 34, 289–305, <https://doi.org/10.1007/s00376-016-6160-5>, 2017.

Wang, Z., Lin, L., Yang, M., and Xu, Y.: The effect of future reduction in aerosol emissions on climate extremes in China, *Clim. Dynam.*, 47, 2885–2899, <https://doi.org/10.1007/s00382-016-3003-0>, 2016.

- 930 Wilks, D.: On “field significance” and the false discovery rate, *J. Appl. Meteorol. Clim.*, 45, 1181-1189, <https://doi.org/10.1175/JAM2404.1>, 2006.
- Xiong, L., Yan, L., Du, T., Yan, P., Li, L., and Xu, W.: Impacts of climate change on urban extreme rainfall and drainage infrastructure performance: a case study in Wuhan City, China, *Irrig. Drain.*, 68, 152-164, <https://doi.org/10.1002/ird.2316>,
935 2019.
- Xu, H., Chen, H., and Wang, H.: Future changes in precipitation extremes across China based on CMIP6 models, *Int. J. Climatol.*, 42, 635-651, <https://doi.org/10.1002/joc.7264>, 2022a.
- 940 Xu, H., Chen, H., and Wang, H.: Detectable human influence on changes in precipitation extremes across China, *Earth's Future*, 10, e2021EF002409, <https://doi.org/10.1029/2021EF002409>, 2022b.
- Xu, K., Xu, B., Ju, J., Wu, C., Dai, H., and Hu, B. X.: Projection and uncertainty of precipitation extremes in the CMIP5 multimodel ensembles over nine major basins in China, *Atmos. Res.*, 226, 122-137,
945 <https://doi.org/10.1016/j.atmosres.2019.04.018>, 2019.
- Yang, X., Zhou, B., Xu, Y., and Han, Z.: CMIP6 evaluation and projection of temperature and precipitation over China, *Adv. Atmos. Sci.*, 38, 817-830, <https://doi.org/10.1007/s00376-021-0351-4>, 2021.
- 950 Yatagai, A., Kamiguchi, K., Arakawa, O., Hamada, A., Yasutomi, N., and Kitoh, A.: APHRODITE: Constructing a long-term daily gridded precipitation dataset for Asia based on a dense network of rain gauges, *Bull. Am. Meteorol. Soc.*, 93, 1401-1415, <https://doi.org/10.1175/BAMS-D-11-00122.1>, 2012.
- Ying, X., Bing, Z., Bo-Tao, Z., Si-Yan, D., Li, Y., and Rou-Ke, L.: Projected flood risks in China based on CMIP5, *Adv. Clim. Change Res.*, 5, 57-65, <https://doi.org/10.3724/SP.J.1248.2014.057>, 2014.
- 955 [Zhang, W., & Zhou, T. \(2020\). Increasing impacts from extreme precipitation on population over China with global warming. *Science Bulletin*, 65\(3\), 243-252. <https://doi.org/10.1016/j.scib.2019.12.002>](https://doi.org/10.1016/j.scib.2019.12.002)
- 960 Zhao, X., Li, H., and Qi, Y.: Are Chinese cities prepared to manage the risks of extreme weather events? Evidence from the 2021.07. 20 Zhengzhou Flood in Henan Province, *SSRN Elect J.*, 4, 3303, <http://dx.doi.org/10.2139/ssrn.4043303>, 2021.

Zhu, J., Huang, G., Wang, X., Cheng, G., and Wu, Y.: High-resolution projections of mean and extreme precipitations over China through PRECIS under RCPs, *Clim. Dynam.*, 50, 4037-4060, <https://doi.org/10.1007/s00382-017-3860-1>, 2018.